Imbalanced moment release within subducting plates during initial bending and unbending

T.J. Craig[1], P. Methley[1,2], D. Sandiford[3]

[1]COMET, Institute of Geophysics and Tectonics, School of Earth and Environment, University of Leeds, Leeds, LS2 9JT, UK.

[2]Department of Earth Sciences, University of Cambridge, Cambridge, CB3 0EZ, UK.

[3]Institute of Marine and Antarctic Studies, University of Tasmania, Tasmania, Australia.

Key Points:

- Intraslab seismicity is localised by the concentration of bending stresses in regions of changing slab geometry (both bending and unbending)
- Generally, more seismic moment is released during bending than unbending, and in intraslab extension rather than intraslab compression
- The modulating influence of inplane stresses on the bending stress field appears to lead to an accumulation of permanent inplane strain

Corresponding author: T.J. Craig, `t.j.craig@leeds.ac.uk`

Abstract

Internal deformation within the downgoing plate in subduction zones to accommodate the bending of the plate as it starts to subduct is reflected in widespread intraplate seismicity. This seismicity, extending from the outer rise and outer trench slope, down to intermediate depths within the slab, is dominated by the combination of both normal- and thrust-faulting earthquakes reflecting the accumulation and recovery of down-dip curvature. In the idealised case, where all internal deformation is recovered and slabs descend as a straight plate into the deeper mantle, we might expect the seismic moment released in both extension and compression to balance. However, a number of factors may complicate this: the thermal, compositional, and rheological evolution of the slab as it subducts, changes in the proportion of deformation accommodated seismically, and whether the slab undergoes any permanent deformation (e.g., slab necking). Here, we assess earthquake moment release in intraslab settings around the world, focusing on those subduction systems with relatively simple slab geometries. Whilst moment balances for individual regions are often heavily dependent on extreme large-magnitude events, considering the combination of numerous regions around the western Pacific and eastern Indian Ocean indicates that substantially more deformation is accommodated seismically during bending than during unbending, and that in both settings, significantly more moment release reflects down-dip extension than down-dip compression. This suggests that, although the location of seismicity is clearly related to changes in slab curvature, there is a component of permanent, unrecovered down-dip extension in many subducting slabs.

Plain Language Summary

As tectonic plates descend into the Earth's interior, they must first bend to start their descent, then unbend as they straighten in the upper mantle. This bending process is accompanied by the occurrence of earthquakes, indicative of brittle failure and the accumulation of long-term strain within the plate. In the ideal case, where the entire bend is reversed, this strain would be expected to be fully recovered, with bending-related seismicity matched by seismicity associated with unbending. Here, we test this simple hypothesis, and find a moment imbalance, with significantly more seismicity associated with the initial bend rather than subsequent unbending, and with significantly more seismic moment release in down-dip extensional seismicity, in both bending and unbending regions, than moment release in down-dip compressional seismicity. This sug-

gests that, although seismicity within the subducting slab strongly correlates with changes in slab curvature, there is also an accumulation of permanent strain, indicative of slab necking, that persists through the bending/unbending process through the changing balance of compression/tension in regions of changing curvature.

1 Introduction

In subduction zones, two tectonic plates come together, and one must bend, buckle, and descend into the Earth's interior. The bending of the incoming plate, associated with the initial development of down-dip curvature, leads to widespread faulting in the outer rise and outer-trench slope regions, with associated seismicity. In the majority of subduction zones, slab curvature continues to increase beneath the forearc, before beginning to reverse as the slab straightens and descends into the Earth's interior. Slab morphology after subduction can be complex, and displays a range of behaviours, from the simple recovery of curvature, leaving a straight slab that descends into the mantle (e.g., Honshu, central Tonga), to complex shallow-slab morphologies, involving flattened slabs and slab tearing (e.g., southern Mexico, Peru). Along-strike curvature can add further complexities, and additional deformation and faulting (e.g., South Sandwich Islands subduction zone, the Hellenic Arc).

The implications of intraslab seismicity remain unclear. There are rheological questions regarding the conditions required to permit seismicity to occur at the depths and pressures seen within slabs. But there are also questions regarding the deformation field that these earthquakes represent. Whilst smaller intraslab earthquakes may be related directly to the release and passage of free fluids (e.g., Halpaap et al. (2019)), larger-magnitude seismicity must be the result of the plate-scale stress field in the source region, and therefore provides a vital insight in to the stress state and geodynamics of the slab, even if the rheological conditions allowing brittle deformation are related to local mineralogy and the occurrence of metamorphic transitions within the slab (e.g., Isacks and Molnar (1971); Peacock (2001); Hacker et al. (2003)).

Initial work analysing the intraslab stress field through earthquake focal mechanisms (e.g., Isacks and Molnar (1969, 1971); Alpert et al. (2012)) suggested that intraslab deformation was dominated by the influence of axial plate stresses (ie., slab pull; ridge push; tractions on the edges of slabs, and lower mantle resistance). In contrast, more re-

cent work, benefiting from better resolution in earthquake locations, suggests that changes in curvature (bending/flexure) provide a first-order explanation for the location and orientation of intraslab seismicity in many global subduction settings (Bailey et al., 2012; Myhill, 2013; Sandiford et al., 2019, 2020). This particularly applies to slabs at shallow depth within the mantle, before interactions with the mid-mantle transition zone at ∼660 km become important. Whilst increasing evidence from the polarisation of double seismic zones (e.g., Igarashi et al. (2001); Kita et al. (2010); Bloch et al. (2018)) and the correspondence between slab seismicity and slab curvature (e.g., Myhill (2013); Sandiford et al. (2020)) suggest that bending stresses dominate in driving intraslab seismicity, the degree to which this interacts and overprints the in-plane stress field remains uncertain.

Here, we test a simple hypothesis: in regions where slab morphology is relatively simple during the initial stages of subduction, with the development and recovery of a single predominant down-dip bend, does the seismic moment released in the development of the bend (increase in curvature) match that released during the unbending process (decrease in curvature)? Below, we outline our approach to isolating seismicity associated with the changing down-dip curvature of slabs, illustrate the application of this approach to 13 relatively simple regions of active subduction, and discuss the implications of the observed moment released through this process for the geodynamics of subduction.

2 Data Analysis

2.1 Seismicity catalogues

Most subduction zones are host to prolific seismic activity associated with various elements of the subduction process (seismicity on the main subduction interface, within the downgoing plate, and within the overriding plate). To isolate a subset of the earthquake catalogue that is associated only with changes in the downdip curvature of the descending plate, we require accurate information on both the location of the earthquake, and the style of deformation that the earthquake represents (exemplified in the moment tensor). In this study, we draw on two seismicity catalogues, with different strengths. We rely on the gCMT catalogue (Dziewonski et al., 1981; Ekström et al., 2012) for information regarding earthquake moment tensors and earthquake magnitudes. However, the relatively long period seismic data upon which the gCMT catalogue relies inhibits

the precise determination of earthquake locations, leading to relatively large uncertainties, particularly in source depth. Instead, we draw on the ISC-EHB catalogue (Engdahl et al., 2020) for locations. This catalogue, reliant on the inversion of phase arrival times for a multitude of phases, offers the most comprehensive and accurate routinely-calculated, global catalogue of earthquake locations available. In combining the two catalogues, we are limited in both the magnitude range we can use, typically determined by the completeness of the gCMT catalogue, and the time duration to the catalogues. Here, we use catalogues extending from 1970 to the end of 2016, the current end date for the ISC-EHB.

To combine these two catalogues, we first take regional subsets of both catalogues, 1° greater in every direction that a given study area, allowing a buffer zone around the edge of our study area such that we avoid the problem of losing events due to small mismatches between catalogue locations around the periphery of a regional study area. The origin time of each catalogue entry is converted to decimal years. We then test every event in the gCMT catalogue against entries in the ISC-EHB catalogue, looking for entries that match within given tolerance in term of origin time ($< 3 \times 10^{-7}$ yrs), inter-catalogue event separation (< 50 km) and magnitude (within 2 magnitude units). Tolerance thresholds are adapted slightly for regional variability, particularly in the location accuracy of larger events in the gCMT catalogue.

To pass through to our final catalogue, we require an entry in the gCMT catalogue to be associated with a single entry in the ISC-EHB catalogue. In cases where two matches exist in the ISC-EHB catalogue to one gCMT entry, we discard the result - this limitation particularly affects events within aftershock sequences, especially after major interface seismicity (e.g., Honshu shortly after the 2011 M_w9.0 Tohoku-Oki earthquake). Discarded results, both those with no matches, and those with multiple potential matches, are checked manually to ensure that no major (large-magnitude) earthquakes are excluded. In general, this approach usually yields matches for $> 95\%$ of earthquakes in the gCMT catalogue.

For each correlated event, we then take the source time and hypocentral location from the ISC-EHB catalogue, and the moment tensor and moment magnitude from the gCMT catalogue, and use this combined catalogue for the rest of the study.

2.2 Region selection and structure

We focus our study on 13 regions, selected on the basis of a relatively simple slab morphology characterised by a single major bend, followed by a relatively straight section of slab at intermediate depth, based on the slab models of G. P. Hayes et al. (2012) and G. Hayes et al. (2018) (hereafter referred to as "Slab1" and "Slab2" respectively). These 13 regions include six regions from the NW Pacific (Aleutians, Kuriles-Kamchatka, Honshu, Ryukyu, Bonin, Marianas), three from the SW Pacific (The Solomon Islands, New Britain, and the New Hebrides), two sections of the Tonga-Kermadec-Hikurangi subduction system (Tonga-Kermadec, Kermadec-Hikurangi), and two from Indonesia and the western Indian Ocean (Sumatra, Java-Sumba). In Figures 1 – 3 we show processing results from three example regions (Honshu, Kuriles-Kamchatka, Tonga-Fiji-Kermadec), and include processing results from the other 10 regions in supplementary material (Figures S2 – S11).

In assessing the relationship between seismicity and slab geometry, we rely on the Slab1 and Slab2 models for the surface of the subducted plate. We note the slight circularity in using models for the slab geometry that are partially derived using earthquake locations (particularly for Slab1) to interpret the geometrical context of the same seismicity. As Slab2 also uses numerous other constraints (e.g., seismic tomography, reflection and refraction data), and as we are interested in the changes in slab morphology, rather than its actual location in space, we consider this circularity to be only a minor concern with this model, and prefer this more recent compilation of slab models. In a limited number of cases, where the regional slab geometry from Slab2 clearly deviates from the location of nearby seismicity (Tonga-Fiji-Kermadec, Bonin), we revert to using the older Slab1 model.

2.3 Earthquake reprojection

To isolate a set of earthquakes limited to intraslab deformation, and to interpret these in the context of the local slab geometry, we need to reproject our earthquake catalogue into a slab-relative reference frame.

For each region, we draw on the plate boundaries of Bird (2003), or, where these visibility deviate from the bathymetric trench, our own determination of the local trench line from available bathymetric data. In relating earthquakes to changes in slab geom-

etry, we reproject our earthquake dataset into a slab-relative reference frame, and for the determination of metrics relating to slab geometry involved in this (dip, curvature and rate-of-change in curvature), we again rely on the chosen regional slab model.

We start by merging the relevant slab model for each region with a flat bathymetry at its up-dip extent, to extend it out onto the oceanic plate. Following the approach of Sandiford et al. (2020), we then determine a set of trench-perpendicular azimuths at 20 km intervals along the plate boundary, and extract the slab geometry along each trench-perpendicular profile. The study area, and seismicity catalogue, is then limited by the two profile lines at either end of the selected region (yellow lines on Figures 1 – 3 and S2 – S11). For each profile line, we determine the slab dip, the down-dip curvature, and the rate of change of curvature down-dip (e.g., Figure 1d,e,f respectively).

Figures 1 – 3 show three example regional study areas, for Honshu, the Kuriles-Kamchatka Arc, and Tonga-Fiji-Kermadec, and cross sections through the slab model and earthquake dataset, with the horizontal axis being distance from the trench. For every earthquake in our combined earthquake catalogue, we associate the earthquake with a profile line based on the closest profile to the earthquake location, when both are projected to the Earth's surface. We then calculate the earthquake location in terms of downdip distance along the slab surface profile, and perpendicular distance from the closest approach to the slab surface (i.e., distance along the slab surface, and depth into the slab; shown in Figures 1 – 3c).

2.4 Isolating intraslab seismicity

Finally, we apply a set of filters aimed at isolating the subset of seismicity which is associated with the down-dip deformation of the slab. In order to be retained, earthquakes are required to pass all of the following filtering stages:

- Earthquakes are required to have a minimal non-double couple component to their moment tensor. Here, we limit this by requiring the percentage double couple (γ) to be $> 70\%$. We follow Jackson et al. (2002) in defining this as:

$$\gamma = 100 \times \left(1 - \left(\frac{3 \times |\lambda_2|}{|\lambda_1| + |\lambda_3|}\right)\right) \tag{1}$$

  where λ_i are the eigenvalues of the moment tensor.

- We exclude all earthquakes where the depth from the ISC-EHB catalogue is shallower than 15 km above the local depth of the slab surface from Slab2 (or Slab1 for the Tonga-Fiji-Kermadec and Bonin regions). For completeness in removing shallow earthquakes within the over-riding plate, we also remove earthquakes at distance landward from the trench where no slab model is present.
- To remove earthquakes associated with motion on the subduction interface, we follow Sandiford et al. (2020) in determining a similarity coeffcient (χ) between the moment tensor of each earthquake, and a predicted subduction interface moment tensor based on the orientation of the local slab surface. We define this similarity as:

$$\chi = \frac{\mathbf{M}_{ij}^{\text{interface}} : \mathbf{M}_{ij}^{\text{eq}}}{||\mathbf{M}^{\text{interface}}||\,||\mathbf{M}^{\text{eq}}||} \tag{2}$$

  where $||\mathbf{M}||$ is the norm of the moment tensor, and : is the tensor double dot product. Here, we predict the interface moment tensor based on the local slab geometry at the location of each earthquake, and assume that interface events are pure dip-slip compressional deformation. Earthquakes that are within 15 km of, or deeper than, the slab surface, and with a χ value above a threshold value are deemed too similar to the expected interface deformation, and excluded. The threshold value of χ is determined manually for each region, based on the χ/frequency distribution, where the interface is marked by the onset of a rapid increase in the number of earthquakes per χ increment as χ approaches 1. We tested an approach where the interface moment tensor was calculated using the slab model geometry and a rake value based on the regional plate motions (allowing a non-dip-slip component to the moment tensor), however this was found to produce less clear χ distributions in cases where subduction is oblique, due to the common partitioning of slip between trench-normal deformation on the interface, and trench-parallel deformation within the forearc (McCaffrey et al., 2000).
- To remove earthquakes associated with strike-slip deformation within the slab, we exclude all earthquakes with a null axis within 45° of the local slab normal vector.
- To remove earthquakes predominantly representing along-strike deformation within the slab, we exclude earthquakes with a null axis within 35° of the local slab dip vector.

- Earthquakes are required to be located up-dip of the first-zero crossing in the curvature of their associated slab profile. This step is aimed as isolating our dataset from complexities in the slab geometry beyond the first initial bend and the recovery of this curvature.
- In certain cases, most notably for Honshu during the aftershock sequence of the 2011 Tohoku-Oki earthquake, we add an additional filter, designed to remove extensional earthquakes within the forearc of the over-riding plate. We exclude earthquakes arc-wards of the trench, between 12.5 and 60 km depth, with depths shallower than the local slab depth, and with T-axes that are closer to vertical than the P-axis.

Figures 1a,b and 2a,b show the impact of applying all of these filters, with all earthquakes excluded by these steps shown in grey, and those retained shown in blue (downdip extension) and red (downdip compression).

3 Regional examples

Figures 1 – 3 show three regional examples of the processing approach described, for northern Honshu, the Kuriles-Kamchatka Arc, and Tonga-Fiji-Kermadec, respectively. Figure 1 shows perhaps the most straightforward example of an initial bend developed through the outer rise and outer trench slope, with pervasive downdip extensional faulting at shallow depth to 30-40 km arc-wards of the trench, which matches the peak in curvature of the slab. This is then followed by a rapid transition to down-dip compressional faulting at shallow depths within the downgoing slab as the curvature is recovered, with some limited down-dip compressional seismicity at greater depth on the outside of the unbend. All intermediate-depth seismicity largely ends by ∼400 km along the slab surface, as the curvature returns to zero. Even in this simple case, however, it is important to note that although the slab geometry and dip are relatively consistent across the study region (Figure 1b,c), as we consider curvature and rate-of-change in curvature, increasingly complex variability emerges, emphasising the need to consider the localised slab geometry along each profile at the location of each earthquake.

Figure 2 also shows a more complex case for the Kuriles-Kamchatka Arc. As demonstrated in Figure 2a,b, the overall slab geometry here is also comparatively simple, dominated in all cases by a single major bend, before straightening out at $\sim$ 200 km depth.

However, increased variability in the along-strike geometry of the slab (Figure 2d,r,f) again emphasises the need to consider each earthquake in its local geometrical context. Once again, we see the initial development of plate curvature expressed through shallow down-dip extensional seismicity. This is accompanied by limited deeper compressional seismicity on the inside of the bend beneath the outer rise (T. J. Craig, Copley, & Jackson, 2014). Around the section of peak curvature, expected to mark the transition from predominant bending to predominant unbending, we see the sudden cessation in down-dip extensional seismicity, and the onset of widespread down-dip compressional seismicity, accompanied by minor down-dip extensional faulting at greater depth into the slab (Figure 2c). During unbending, as the plate returns to zero-curvature, seismicity is separated into shallow down-dip compression and deeper down-dip extensional zones, as in the majority of the western Pacific margin slabs (Sandiford et al., 2020). Matching detailed studies of the depth extent of seismicity in outer rise regions around the world (T. J. Craig, Copley, & Jackson, 2014), we expect the complete separation between extensional and compressional seismicity, and, in the absence of any exterior variation in the stress field, a consistent depth of the separation between the two. The slight overlap seen on Figure 2c suggests that either the resolution in earthquake locations available from the ISC-EHB catalogue, the resolution of the slab model, or a combination of the two slightly obscures the finer details of the transition between deformational regimes with depth into the slab.

In Figure 3 we show a more complex example, which highlights a number of remaining limitations. This region - the northern end of the Tonga-Fiji-Kermadec subduction system - is one of the most active intraslab settings in the world, with high productivity rates of both intermediate depth and deep-focus seismicity. The first limitation is the reliance on existing slab models. In this case, when using Slab2 (Figure S1) there is a clear spatial deviation between the intraslab seismicity, and the slab surface, with the slab model consistently underestimating slab dip (or the seismicity being consistently mislocated), leading to a progressive increase in depth-within-slab with distance along slab. In the example shown in Figure 3, we instead use Slab1 (G. P. Hayes et al., 2012) as the slab model. In this case, we make this choice based on a clear divergence between the location of intraslab seismicity (from the ISC-EHB catalogue), and the slab location in Slab2 (shown in Figure S1). Comparing Figure 3 and Figure S1, the overall slab shape, the variation in slab curvature, and the location of inflection points in slab curvature are

broadly similar, but while the slab depth (integrated dip) in the case of Slab2 is consistently less than would be predicted by the location of seismicity, Slab1 (more directly constrained by seismicity) produces a slab top that is much more consistent with the location of intraslab seismicity, as highlighted by the two slab relative cross sections. A similar deviation is only seen for two other regions (Bonin, Kermadec), when Slab2 similarly under-predicts the depth of the slab. In these cases, we again revert to Slab1.

The second limitation, connected to the first, is the reliance on slab models in limiting the down-dip extent of the seismicity considered. In both Figures 2a and 3a, small groups of events are included in our summation, substantially further down-dip than the cut-off limit imposed for most of the subduction zone (at 150°E, 50.5°N and -178°E, -22 – -20°N respectively). This is again a result of method described above, where the depth range over which the slab model indicates unbending (i.e. where the downdip curvature remains positive, prior to returning to zero) can vary substantially. This is in keeping with the approach described above, and technically correct, but again highlights a potential problem in cases where the slab geometry is either not well defined, or complex. This potential uncertainty is notably absent for the simple slab geometry under Honshu (Figure 1). In contrast, the increasingly complex geometries of the Kuriles-Kamchatka (Figure 2d-f) and Tonga-Kermadec (Figure 3d-f) cause such issues to arise, although the moment contribution from such earthquakes is comparatively small.

Despite these issues, Figure 3 shows a broadly similar pattern of seismicity to Figure 2, with the clear separation of shallow down-dip extension and deeper down-dip compression in the outer rise, switching to shallow down-dip compression and deeper down-dip extension at intermediate depths. Whilst absolute separation is again not imaged using our combined earthquake catalogue, more detailed studies of the outer rise region along Tonga-Kermadec have shown that this is the case seaward of the trench (Lay et al., 2013; Todd & Lay, 2013; T. J. Craig, Copley, & Jackson, 2014), and we see no reason why it would not persist at greater depths.

All three regional examples also show the composite moment tensors from summing all down-dip extensional (g) and down-dip compressional (h) earthquakes, after rotation into a slab-relative reference frame, along with stereonet plots of the P, N, and T axes for the relevant earthquake selections. In each of the three cases shown, the composite mechanisms for down-dip extensional and down-dip compressional seismicity have sim-

ilar orientations, supportive of the concept that faults initiated during the initial development of the bend are reactivated at intermediate depth with the opposite sense of motion (Chen et al., 2004; Ranero et al., 2005).

Whilst we show only three of our 13 regional studies in this manuscript, we include similar plots for the other regional studies in supplementary material (Figures S2 – S11).

4 Moment summation

Our intention in this study is to consider the deformation accommodated seismically during the initial flexural cycle (bending and unbending) as the downgoing plate enters the subduction zone. We have therefore limited the seismicity catalogue considered to only earthquakes located up-dip of the first zero-crossing in the curvature of each slab profile, in effect, the point where the slab geometry first returns to being "straight" (shown by the solid purple lines of Figures 1c,e and 2c,e). The total flexural deformation between the oceanward extent of deformation and this point should sum to zero (when considering both strain accommodated both seismically and aseismically). We then further subdivide the seismicity catalogue, using two methods to assign earthquakes to regions of "bending" and regions of "unbending". In the first, we determine the point of maximum curvature on each profile, and assign earthquakes up-dip of this point as "bending", and down-dip as "unbending". In the second, we instead assign earthquakes based on the rate of change in curvature (Figures 1f, 2f); earthquakes located where the calculated rate of change in curvature is positive are designated to be related "bending", and those corresponding to negative values designated to be related to "unbending". We also consider further separation into earthquakes related to down-dip extension, and those related to down-dip compression, based on the orientation of the P and T axes with respect to the slab dip vector. Note that, whilst we illustrate these divisions in figures 1 and 2 using the mean slab profiles, the point of peak curvature, and the rate-of-change of curvature are calculated for each profile, with each earthquake using the values from their closest associated profile.

In a number of cases (e.g., Aleutians, Figure S2; Solomons Figure S6), we note that the slab models used resort to a flat slab with zero dip at depth, due to a paucity of data. This could, in theory, lead to an under-estimation of the first down-dip return to zero curvature, and lead to the exclusion of some earthquakes that would otherwise be clas-

sified as "unbending". However, this lack of constraint is partly due to a lack of earthquakes, and hence both in general, and in the specific regions we consider here, we do not consider this to a problem for our analysis.

In Figure 4, we show the results for the moment summation of all 13 regions considered here. In each region, we sum earthquakes by their relation to regions of bending and unbending (in the case of Figure 4, on the basis of the rate of change in curvature), and also separate by mechanism type. We also highlight in each case the contribution of the largest earthquake which each grouping, shown by the white bars. In many cases, the moment release is dominated by one major event (e.g., the M_w 8.3 1977 Sumba earthquake for the Java region; the M_w 7.9 2014 Rat Islands earthquake for the Aleutian Arc) - a problem which limits the extent to which the overall deformation state of any given slab, when taken in isolation, can be assessed from our available earthquake catalogues, which may not be entirely representative of the long term deformation pattern.

Figure 4 shows summations using the rate-of-change in curvature to separate earthquakes into regions of bending and unbending. In Figure S12, we show an equivalent set of summations where we instead define this separation based on whether earthquakes are updip of the point of maximum curvature on the closest slab profile to the earthquake location, or between the point of maximum curvature and the first subsequent zero-curvature point. As these figures show, this different method of separation makes little difference to the majority of regions. The only major changes are for Ryukyu and the New Britain subduction zone, where the different definition changes the moment balance between unbending and bending, because the largest earthquake in the population changes from bending to unbending (or the inverse).

Most individual regions we consider are subject to sampling bias, given both the dominance of a small number of individual events, and that, with only a 46-year catalogue duration, we are looking at a relatively small portion of the seismic cycle in such regions. Hence, instead of further interrogating individual regions, we combine our regional catalogues into a single composition catalogue. Individual regions differ in a number of crucial ways, including different rates of subduction and degree of curvature, leading to differing strain rates; differing seismogenic thicknesses; differing geodynamic settings.

Of the 13 regions we consider, and show on Figure 4, we exclude one, Sumatra (Figure S10), from further consideration. Sumatra shows a notably different pattern in intraplate seismicity, with the shift from seismicity evidencing bending to seismicity suggesting unbending, occurring slightly seawards of the trench (T. Craig & Copley, 2018) – significantly further up-dip than in any other subduction zone, and in a manner that does not entirely match the long-term strain implied by the geometry of the plate interface (Singh et al., 2012). This notably different behaviour of the intraslab seismicity may be a result either of a dynamically-evolving overriding plate, effecting the near-trench intraslab stress field (T. Craig & Copley, 2018), or a consequence of the diffuse intraplate deformation occurring seawards of the trench within the Indian Ocean, to accommodate the differential motion of India with respect to Australia (e.g., Wiens et al., 1985; Geersen et al., 2015). We therefore exclude it from our further compilation.

Figure 5 shows the summation of moments from all 12 remaining regions from Figure 4. Again, the white bars show the contribution of the largest event to each bin (with the largest single event being the M_w 8.3 1977 Sumba earthquake). The upper panel shows the results when earthquakes are divided based on the rate of change in curvature at the location of each earthquake, the lower panel when they are separated based on whether they are up-dip or down-dip of the maximum curvature point on their associated profile. Again, the different mechanism of defining the separation from bending to unbending makes little difference to the overall moment balance. Two observations stand out, regardless of which separation approach is used.

Firstly, substantially more seismic moment is released in the initial bending process than in the recovery of the same total curvature. Given that, as slabs descend into the mantle, they will heat up, their seismogenic thickness decreases, and increasing amounts of strain will be accommodated through ductile deformation, this seems reasonable. However, the majority of the cases considered here are old, cold subducting plates, where the internal seismogenic structure is unlikely to evolve rapidly during the initial phases of subduction. This variation is potentially more likely to derive from the requirement for deeper earthquakes to occur in regions where the evolving mineralogical composition of the subducting plate leads to the release of fluid, permitting seismogenic failure to occur.

Secondly, in all cases, moment release through earthquakes accommodating down-dip extension is significantly higher than that released in earthquakes accommodating down-dip compression. Whilst it remains subject to sampling problems related to the dominance of the largest individual earthquake, this latter trend also holds for all of the individual regions studied (Figure 4), with the exception of Bonin. This asymmetry is most pronounced in the initial bending region, in line with expectations that both supported stresses likely increase with depth, and that the ductile lithosphere can support a small proportion of the total stress.

5 Geodynamic implications

Inferring geodynamic processes (fundamentally dependent on stress and strain) from moment release can be a complex process. Following Kostrov (1974), moment release from a population of earthquakes can be related to volumetric strain (ϵ_{ij}) using:

$$\epsilon_{ij} = \frac{1}{2\mu V} \sum_{k} M^{k}_{0,ij} \tag{3}$$

where V is the volume under consideration and μ is the shear modulus, under the assumption that all strain is accommodated seismically. In the context of subducting slabs, both the shear modulus and the volume (in effect, the seismogenic cross section of the slab) under consideration will vary with depth as the rheology of the slab evolves as it descends into the Earth's interior, and is subject to increased pressures and temperatures. Exactly how these parameters vary will be different in different slabs, depending on their geometry and the thermo-chemical structure of the incoming plate. However, broadly speaking, we expect the shear modulus to increase slightly with increasing down-dip distance from the trench, and the volume to decrease slightly with distance from the trench, as the plate heats up. In the majority of cases considered here, however, where slabs are usually old and cold at the point of subduction, these effects are likely to be minimal over the depth range we consider.

The narrow vertical separation of regions in horizontal extension and compression in outer rises (T. J. Craig, Copley, & Jackson, 2014) suggests that the elastic core of a bending tectonic plate is relatively narrow ($\lesssim$ 5 km). However, the extent of this elastic core will vary with the elastic limits of the material, and whilst estimates of the effective coefficient of friction on intraplate oceanic faults suggest that this is low (T. J. Craig,

Copley, & Middleton, 2014), it will increase with increasing depth and confining pressure, suggesting that the elastic core would widen to some degree with increasing depth, again potentially decreasing the amount of strain, and related moment release, that is accommodated though permanent seismogenic deformation.

The depth of the transition from down-dip compression to down-dip extension will also change between regions of bending and unbending, as the bending-related stresses are superimposed on any in-plane stresses arising from additional plate-driving and resisting forces (e.g., slab-pull, ridge push). In the regions considered here, with the exception of south of Ryukyu, and potentially northernmost Tonga, the depth of this transition in the outer rise region is over half way to the depth of the brittle to ductile transition (T. J. Craig, Copley, & Jackson, 2014). In the perhaps simplistic view that bending strain is linearly proportional to plate-perpendicular distance from the elastic core, and following Eq. 3, this matches with a greater predicted moment release in the bending region through down-dip extension than through down-dip compression - consistent with the results shown in Figure 5. In the absence of in-plane stresses, unbending should result in the complete reversal of accumulated strain, and would be matched by a mirrored moment release. To explain the greater extensional moment release through unbending as well as bending implies the addition of in-plane stresses which, averaged over all regions considered, are down-dip extensional.

Thus, the dominance of moment release through down-dip extensional earthquakes over down-dip compression throughout the initial curvature cycle indicates that, although the pattern and along-dip distribution of seismicity is strongly related to changes in the plate curvature (Myhill, 2013; Sandiford et al., 2020), a portion of the deformation that takes place in these regions is unrelated to the bending of the slab, but is instead unrecovered down-dip extension indicative of slab necking. That this permanent deformation seems to take place in regions of increased change in curvature suggests that the additional stresses associated with slab bending are necessary to push the slab beyond its elastic limit and into the regime of brittle failure, and that in-plane forces (e.g., slab pull) whilst modulating the depth of the transition between bending stress regimes, are insufficient alone to produce intraslab seismicity. This pattern is consistent with the observation that mature oceanic lithosphere is generally able to support the stresses transmitted from subducted slabs without undergoing significant deformation (i.e. necking instability).

Figure 6 shows a simple conceptual model for the accumulation of permanent down-dip deformation through the recovered bending cycle through the superposition of a down-dip in-plane stress, moving the neutral fibre down (in the bending case) and up (in the unbending case). The change in the depth of neutral fibre that results from the addition of an in-plane stress leads to the bending strain field being different to the unbending strain field, and allows the accumulation of unrecovered strain. In the idealised example shown, the strain resulting purely from the in-plane stress could be accommodated elastically, in the absence of any bending stresses, and therefore would not be expected to produce seismicity in a straight section of slab. The sensitivity of the neutral plane depth is itself dependent on the strength profile of the subducted lithosphere – the lower the yield stress of the plate, the greater the sensitivity of the neutral plane depth will be to variation in the in-plane stress, and the more profound the effect on the accumulation of permanent deformation will be.

Despite the improved resolution in earthquake locations available from the ISC-EHB catalogue, we are typically unable to image accurately the separation between upper and lower seismic zones through bending regions. To do so requires either detailed teleseismic analysis not yet routinely undertaken (e.g., Florez and Prieto (2019); T. J. Craig (2019)), or high-quality local seismic data not globally available (e.g., Wei et al. (2017); Sippl et al. (2018)). However, our results suggest that we would, in general, see a upward-migration in the depth within the plate of the elastic core upon moving from initial bending to initial unbending (note that, due to the summation approach used here, this may not be the case in all subduction regions considered, but we expect to be the case in the majority of regions). Again, we emphasise that the results shown in Figure 5, on which this interpretation is based are drawn from the combination of multiple regions, in which the stress state of the whole slab will vary. The scenario we describe appears to be the average case, but we do not expect this to necessarily apply in all subduction zones when considered individually (it is, for example, not the case for Tonga-Kermadec; see Figure 4).

This discussion has focused on the seismic expression of intraplate strain, but this is only part of the total intraplate strain, and significant strain is accommodated within the plate through ductile deformation of material at higher temperatures. However, the onset of ductile deformation occurs at sufficiently low stresses that we consider the contribution these make to the overall support of the intraplate stress field to be negligible.

Ductile strain is excluded from Figure 6, which focuses on deformation in areas potentially capable of producing earthquakes. In the future, as our understanding of the rheology of subducting plates, and our observational seismic catalogue, develop, it may be possible to construct geodynamic models for the subduction process which can determine the ways in which stress is supported in the slab through both brittle and viscous processes, and to more directly relate modelled estimates of volumetric strain to the distribution of seismicity.

6 Conclusions

Seismicity within subducting slabs is predominantly concentrated in areas of the slab where the down-dip slab curvature is rapidly changing, suggesting slab bending stresses exert a strong first order control on the location of intraslab earthquakes. Here, we have studied the intraslab seismcity associated with a number of subduction zones around the western Pacific and eastern Indian Ocean, where down-dip slab geometries are relatively simple, characterised by the development and recovery of a single major down-dip bend. The shallow intraslab seismicity associated with this first bend and subsequent unbending demonstrates that there is significantly more moment released in down-dip tensional intraslab seismicity than in down-dip compressional earthquakes, in the initial regions of bending and unbending. This imbalance in moment release across the cycle of the initial slab bending indicates that, overall, slabs are undergoing a degree of permanent down-dip extension, consistent with models of (mild) slab necking. We propose a model wherein this accumulation of permanent down-dip strain arises from the variation in the depth within the slab of the neutral fibre associated with each bend, resulting from the superposition of down-dip intraslab stresses on the bending stresses. The down-dip stress alone is usually insufficient to produce brittle failure in the slab, but can act to modulate the depth of the transition between bending and unbending, leading to the accumulation of permanent strain from low intraslab stresses.

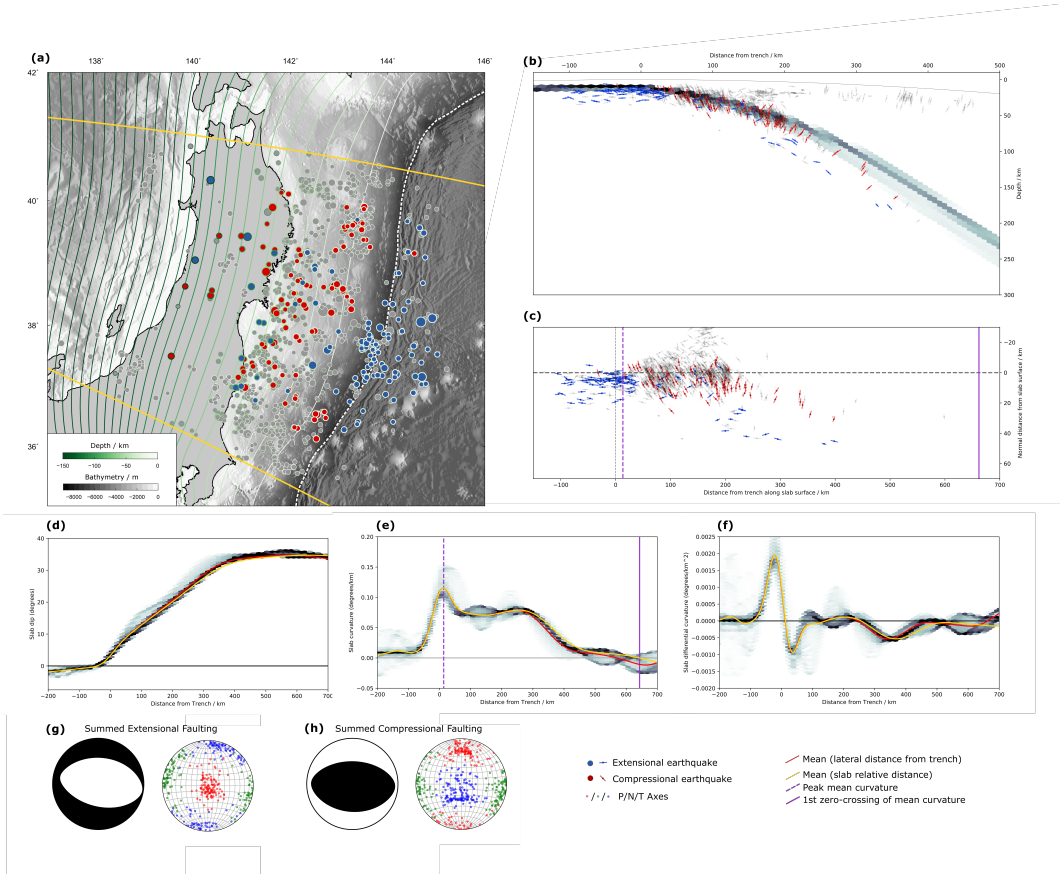

Figure 1. Example processing results from northern Honshu. (a) Map of study area. White-green contours show slab depth from Slab2, and our digitised trenchline (dashed). Yellow lines show the along-strike extent of the the study area. Circles show earthquakes in out combined catalogue, scaled according to earthquake magnitude. Circle outlines are shaded by slab depth. Blue points are down-dip extensional earthquakes updip of the first zero-crossing in curvature. Red points are down-dip compressional earthquakes updip of the first zero-crossing in curvature. Grey earthquakes are those excluded from our catalogue, as discussed in section 2.4. (b) Slab cross section. Earthquakes are shown by the orientation of the tensional axis of the focal mechanism, shaded as in (a). The slab model is shown as a histogram, based on the discrete profiles used in our reprojection scheme, spaced at 10 km. (c) Slab-relative cross section. Earthquakes are plotted as function of down-dip distance and depth-into-slab. T-axes are rotated to be slab relative. (d) Histogram of slab dip as a function of distance. Red line shows the mean slab dip. The yellow line shows mean slab dip, converted into distance along the slab surface. (e) As in (d), but for slab curvature. Purple lines show the maximum in mean curvature in slab-relative distance (dashed line), and the first zero crossing in mean curvature in slab relative distance (solid line). (f) as in (d), but for rate-of-change of slab curvature. (g) Combined mechanism from the summation of all down-dip extensional faulting updip of the first zero-crossing in slab curvature, and a stereonet showing the distribution of P/N/T axes for those earthquakes. Both are expressed in a slab-relative coordinate system. (h) as in (g), but for all down-dip compressional earthquakes.

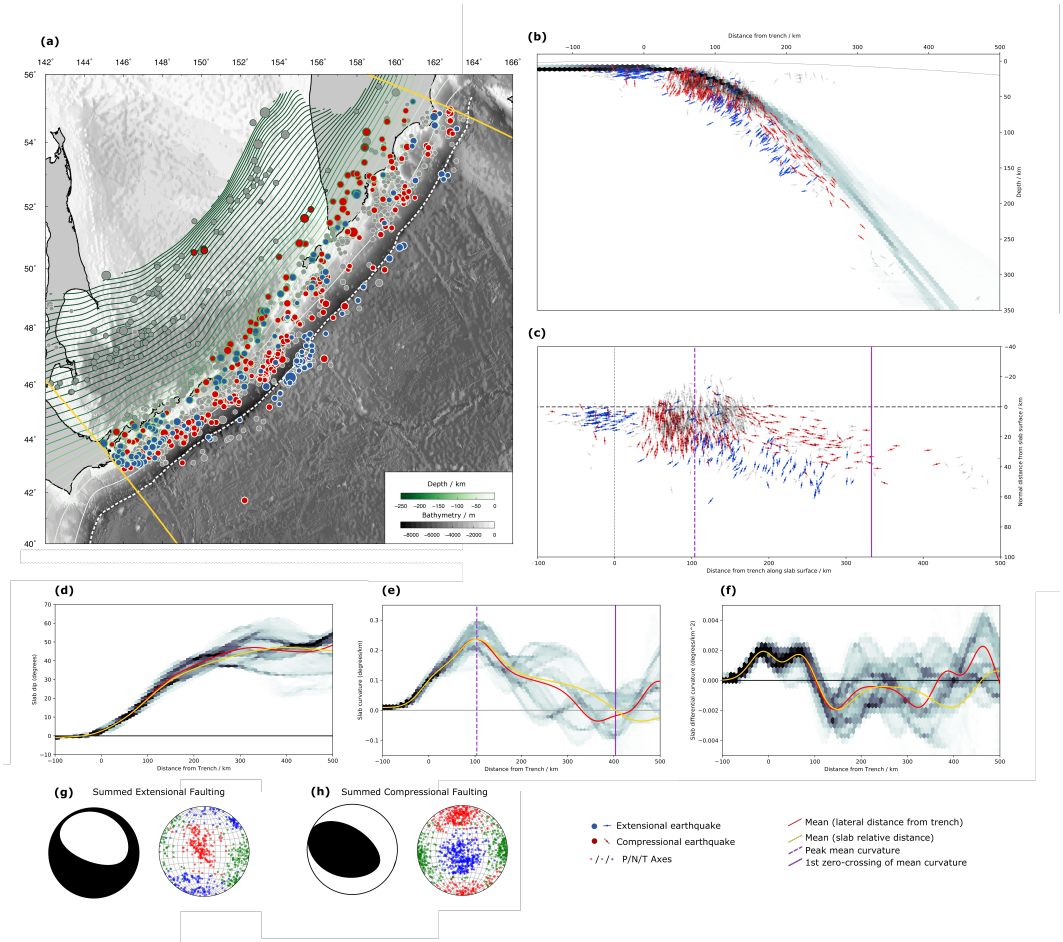

Figure 2. Example processing results for the Kuriles-Kamchatka subduction zone. All plots are as in Figure 1.

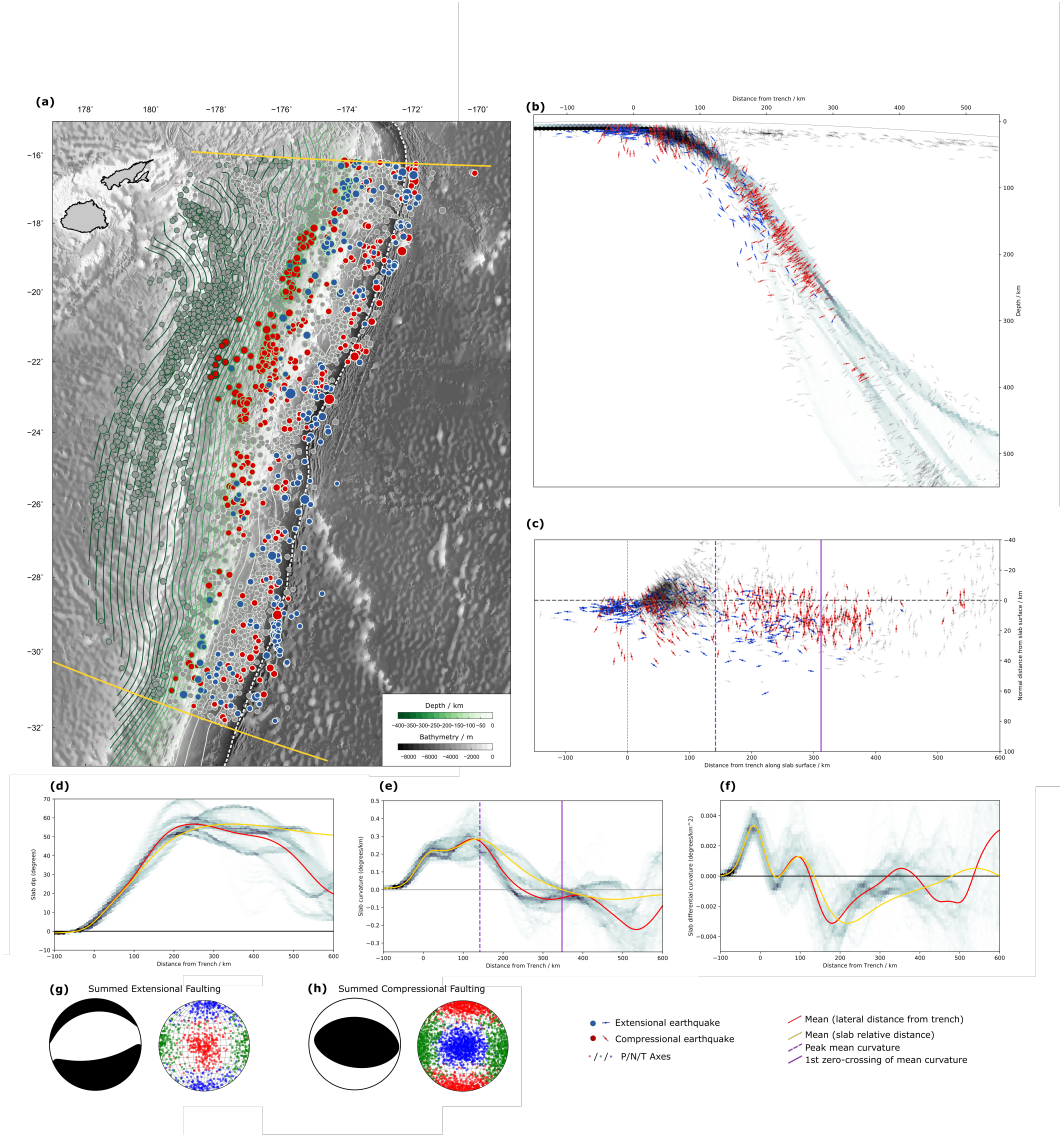

Figure 3. Example processing results for the northern Tonga-Kermadec subduction zone. All plots are as in Figure 1. Note that for Tonga-Kermadec, we use Slab1, not Slab2.

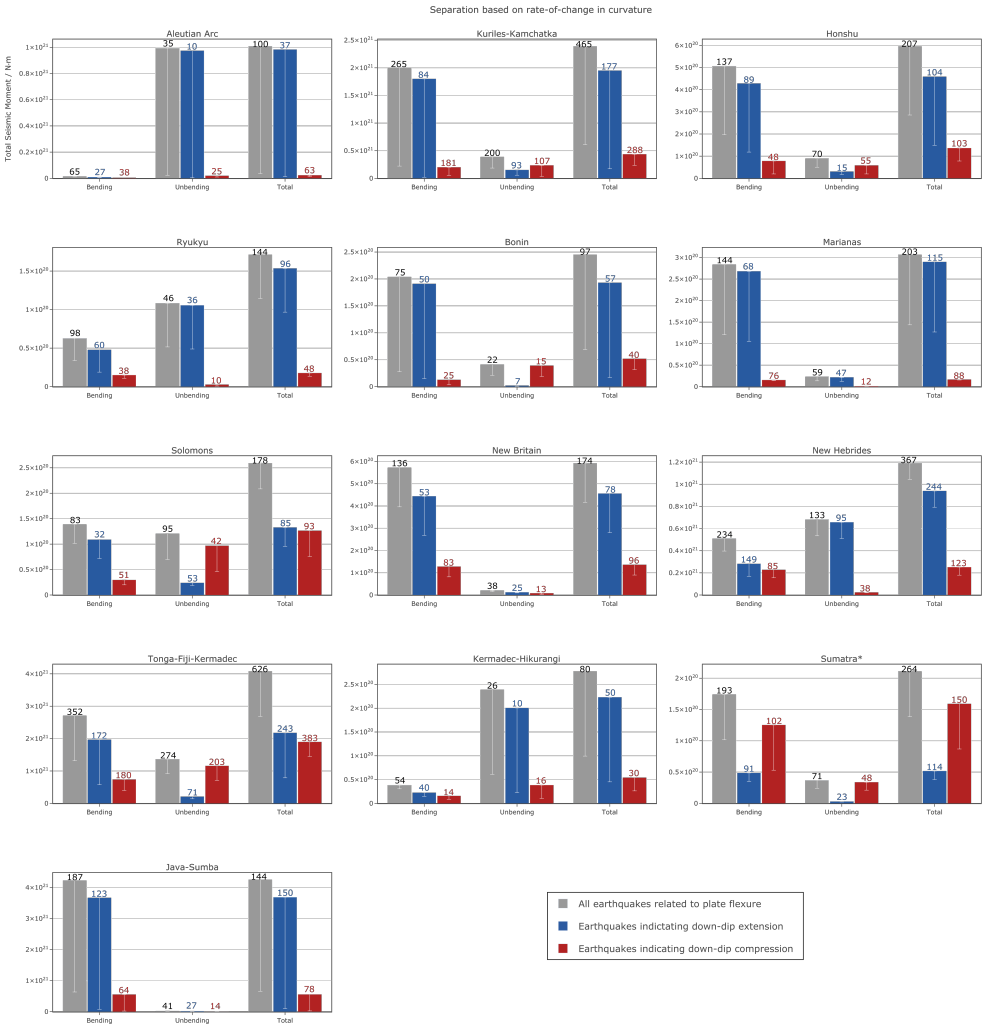

Figure 4. Histograms showing moment summation results for all regions considered. White bars show the contribution of the largest-magnitude earthquake in each bin. Separation into bending and unbending regions is base on the rate-of-change of slab curvature at the location of each earthquake. Numbers above each column indicate the number of earthquakes included in that column. *Sumatra is excluded from Figure 5.

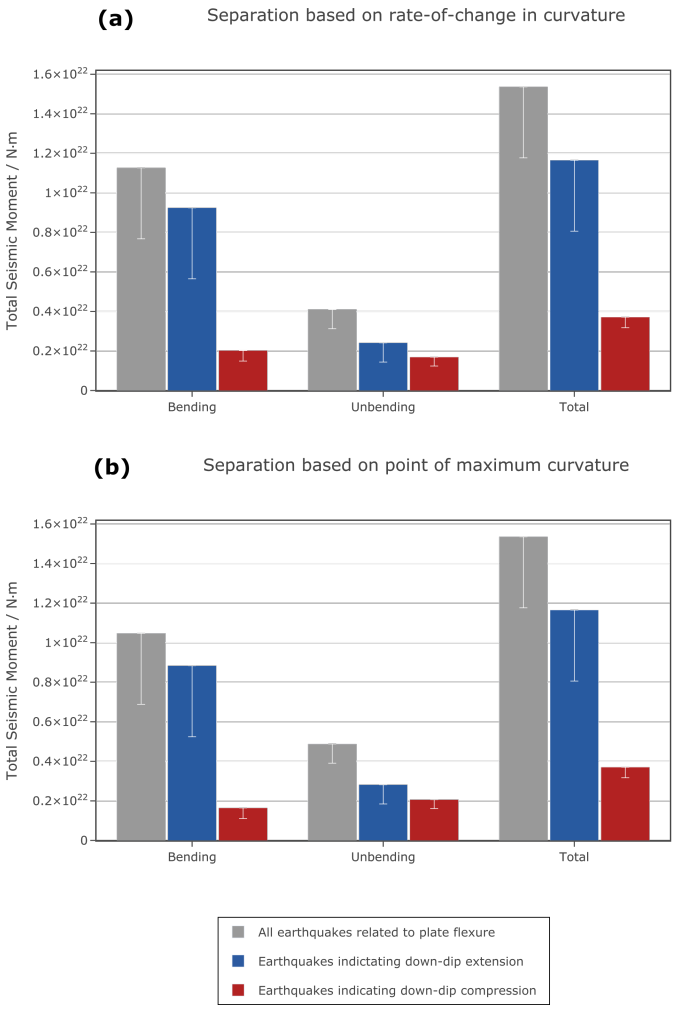

Figure 5. Histograms showing the summed seismic moments from all regions (excluding Sumatra). White bars show the contribution of the largest-magnitude earthquake in each bin. Upper panel shows the summation where earthquakes are split based on the rate of change of curvature. Lower panel shows the summation where earthquakes are split based on their location relative to the point of maximum curvature on their associated slab profile.

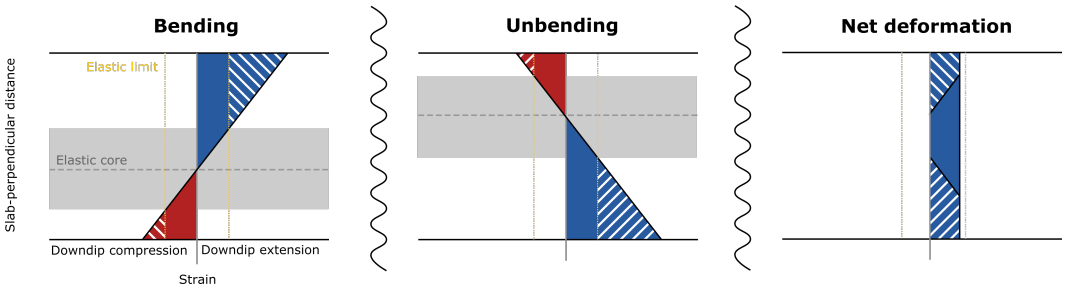

Figure 6. Simplified sketch illustrating how strain imbalance may be achieved through addition of an in-plane stress, superimposed on bending stresses. Red indicates down-dip compression, blue indicates down-dip extension. Crosshatched areas show strain accommodated through permanent (ie., non-elastic) deformation likely to be seismogenic if conditions allow. Grey shaded area shows the elastic core separating areas of potentially-brittle failure. Yellow dashed line shows the elastic limit on strain, assumed to be depth-independent in this conceptual model.

Acknowledgments

TJC and PM were supported in this work by the Royal Society under URF\R1\180088. TJC was also supported through COMET, the UK Natural Environment Research Council's Centre for the Observation and Modelling of Earthquakes, Volcanoes, and Tectonics. We thank Andrew Walker for useful discussions. All data used in this work are freely available from the gCMT project (`https://www.globalcmt.org/CMTsearch.html`), from the ISC (`http://www.isc.ac.uk/isc-ehb/`), and from the USGS (`https://www.sciencebase.gov/catalog/item/5aa1b00ee4b0b1c392e86467/`), all last accessed on 5/10/2020.

References

Alpert, L. A., Becker, T. W., & Bailey, I. W. (2012). Global slab deformation and centroid moment tensor constraints on viscosity. *Geochemistry, Geophysics, Geosystems*, *11*. doi: 10.1029/2010GC003301

Bailey, I. W., Alpert, L. A., Becker, T. W., & Miller, M. S. (2012). Co-seismic deformation of deep slabs based on summed CMT data. *Journal of Geophysical Reearch*, *117*. doi: 10.1029/2011JB008943

Bird, P. (2003). An updated digital model of plate boundaries. *Geophysics, Geochemistry, Geosystems*, *4*. doi: 10.1029/2001GC000252

Bloch, W., Schurr, B., Kummerow, J., Salazar, P., & Shapiro, S. A. (2018). From Slab Coupling to Slab Pull: Stress Segmentation in the Subducting Nazca Plate. *Geophysical Research Letters*, *45*, 5407-5416. doi: 10.1029/2018GL078793

Chen, P.-F., Bina, C. R., & Okal, E. (2004). A global survey of stress orientations in subducting slabs as revealed by intermediate-depth earthquakes. *Geophysical Journal International*, *159*, 721-733. doi: 10.1111/j.1365-246X.2004.02450.x

Craig, T., & Copley, A. (2018). Forearc collapse, plate flexure, and seismicity within the downgoing plate along the Sunda Arc west of Sumatra. *Earth and Planetary Science Letters*, *484*, 81-91. doi: 10.1016/j.epsl.2017.12.004

Craig, T. J. (2019). Accurate Depth Determination for Moderate-Magnitude Earthquakes Using Global Teleseismic Data. *Journal of Geophysical Research*, *124*. doi: 10.1029/2018JB016902

Craig, T. J., Copley, A., & Jackson, J. (2014). A reassessment of outer-rise seis-

micity and its implications for the mechanics of oceanic lithosphere. *Geophysical Journal International*, *197*, 63-89. doi: 10.1093/gji/ggu013

Craig, T. J., Copley, A., & Middleton, T. A. (2014). Constraining fault friction in oceanic lithosphere using the dip angles of newly-formed faults at outer rises. *Earth and Planetary Science Letters*, *392*, 94-99. doi: 10.1016/j.epsl2014.02.024

Dziewonski, A., Chou, T.-A., & Woodhouse, J. (1981). Determination of earthquake source parameters from waveform data for studies of global and regional seismicity. *Journal of Geophysical Research*, *86*, 2825-2852.

Ekström, G., Nettles, M., & Dziewonski, A. (2012). The global CMT project 2004-2010: Centroid-moment tensors for 13,017 earthquakes. *Physics of the Earth and Planetary Interiors*, *200-201*, 1-9. doi: 10/1016/j.pepi.2012.04.002

Engdahl, E., Di Giacomo, D., Sakarya, B., Bkarlaouni, C. G., Harris, J., & Storchak, D. A. (2020). ISC-EHB 1964-2016, an improved Data Set for Studies of Earth Structure and Global Seismicity. *Earth and Space Science*, *7*. doi: 10.1029/2019EA000897

Florez, M. A., & Prieto, G. A. (2019). Controlling Factors of Seismicity and Geometry in Double Seismic Zones. *Geophysical Research Letters*, *46*, 4174-4181. doi: 10.1029/2018GL081168

Geersen, J., Bull, J., McNeill, L., Henstock, T., Gaedicke, C., Chamot-Rooke, N., & Delescluse, M. (2015). Pervasive deformation of an oceanic plate and relationship to large > M_w 8 intraplate earthquakes: The northern Wharton Basin, Indian Ocean. *Geology*, *43*, 359-362. doi: 10.1130/G36446.1

Hacker, B. R., Peacock, S. M., Abers, G. A., & Holloway, S. D. (2003). Subduction Factory 2: Are intermediate-depth earthquakes in subducting slabs linked to metamorphic dehydration reactions? *Journal of Geophysical Research*, *108*. doi: 10.1029/2001JB001129

Halpaap, F., Rondenay, S., Perrin, A., Goes, S., Ottemöller, L., Austrheim, H., ... Eeken, T. (2019). Earthquakes track subduction fluids from slab source to mantle wedge sink. *Science Advances*, *5*. doi: 10.1126/sciadv.aav.7369

Hayes, G., Moore, G., Portner, D., Hearne, M., Flamme, H., Furtney, M., & Smoczyk, G. (2018). Slab2, a comprehensive subduction zone geometry. *Science*. doi: 10.1126/science.aat4723

Hayes, G. P., Wald, D. J., & Johnson, R. L. (2012). Slab1.0: A three-dimensional model of global subduction zone geometries. *Journal of Geophysical Research*, *117*. doi: 10.1029/2011JB008524

Igarashi, T., Matsuzama, T., Umino, N., & Hasegawa, A. (2001). Spatial distribution of focal mechanisms for interplate and intraplate earthquakes associated with the subducting Pacific plate beneath the northeastern Japan arc: A triple-planed deep seismic zone. *Journal of Geophysical Research*, *106*, 2177-2191.

Isacks, B., & Molnar, P. (1969). Mantle earthquake mechanisms and the sinking of the lithosphere. *Nature*, *223*, 1121-1124.

Isacks, B., & Molnar, P. (1971). Distribution of Stresses in the Descending Lithosphere from a Global Survey of Focal-Mechanism Solutions of Mantle Earthquakes. *Reviews of Geophysics and Space Physics*, *9*, 103-175.

Jackson, J., Priestley, K., Allen, M., & Berberian, A. (2002). Active tectonics of the South Caspian Basin. *Geophysical Journal International*, *148*, 214-245.

Kita, S., Okada, T., Hasegawa, A., Nakajima, J., & Matsuzawa, T. (2010). Existence of interplane earthquakes and neutral stress boundary between the upper and lower planes of the double seismic zone beneath Tohoku and Hokkaido, northeastern Japan. *Tectonophysics*, *496*, 68-82. doi: 10.1016/j.tecto.2010.10.010

Kostrov, B. (1974). Seismic moment, and energy of earthquakes, and the seismic flow of rock. *Izvestiya, Physics of the Solid Earth*, *50*, 23-44.

Lay, T., Duputel, Z., Ye, L., & Kanamori, H. (2013). The December 7, 2012 Japan Trench intraplate doublet (M_W 7.2, 7.1) and interactions between near-trench intraplate thrust and normal faulting. *Physics of the Earth and Planetary Interiors*, *220*, 73-78. doi: 10.1016/j.pepi.2013.04.009

McCaffrey, R., Zwick, P., Bock, Y., Prawirodirdjo, L., Genrich, J., Stevens, C., ... Subarya, C. (2000). Strain partitioning during oblique plate convergence in northern Sumatra: Geodetic and seismoogical constraints and numerical modelling. *Journal of Geophysical Research*, *105*, 28363-28376. doi: 10.1029/1999JB900362

Myhill, R. (2013). Slab buckling and its effect on the distributions and focal mechanisms of deep-focus earthquakes. *Geophysical Journal International*, 837-853. doi: 10.1093/ji/ggs054

Peacock, S. M. (2001). Are the lower planes of double seismic zones caused by serpentine dehydration in subducting oceanic mantle? *Geology*, *29*, 299-302.

Ranero, C. R., Villaseñor, A., Morgan, J. P., & Weinrebe, W. (2005). Relationship between bend-faulting at trenches and intermediate-depth seismicity. *Geochemistry, Geophysics, Geosystems*, *6*. doi: 10.1029/2005GC0009972

Sandiford, D., Moresi, L., Sandiford, M., Farrington, R., & Yang, T. (2020). The Fingerprints of Flexure in Slab Seismicity. *Tectonics*, *39*. doi: 10.1029/2019TC005894

Sandiford, D., Moresi, L., Sandiford, M., & Yang, T. (2019). Geometric controls on flat slab seismicity. *Earth and Planetary Science Letters*, *527*. doi: 10.1016/j.epsl.2019.115787

Singh, S. C., Chauhan, A. P. S., Calvert, A. J., Hananto, N. D., Ghosal, D., Rai, A., & Carton, H. (2012). Seismic evidence fo bending and unbending of subducting oceanic crust and the presence of mantle megathrust in the 2004 Great Sumatra earthquake rupture zone. *Earth and Planetary Science Letters*, *321-322*, 166-176. doi: 10.1016/j.epsl.2012.01.012

Sippl, C., Schurr, B., Asch, G., & Kummerow, J. (2018). Seismicity structure of the northern Chile forearc from >100,000 double-difference relocated hypocenters. *Journal of Geophysical Research*, *123*, 4063-4087. doi: 10.1002/2017JB015384

Todd, E. K., & Lay, T. (2013). The 2011 Northern Kermadec earthquake doublet and subduction zone faulting interactions. *Journal of Geophysical Research*, *118*, 1-13. doi: 10.1029/2012JB009711

Wei, S., Wiens, D. A., van Keken, P. E., & Cai, C. (2017). Slab temperature controls on the Tonga double seismic zone and slab mantle dehydration. *Science Advances*, *3*. doi: 10.1126/sciadv.1601755

Wiens, D. A., DeMets, C., Gordon, R. G., Stein, S., Argus, D., Engeln, J., ... Woods, D. (1985). A diffuse plate boundary model for Indian Ocean tectonics. *Geophysical Research Letters*, *12*, 429-432.

Figure 1.

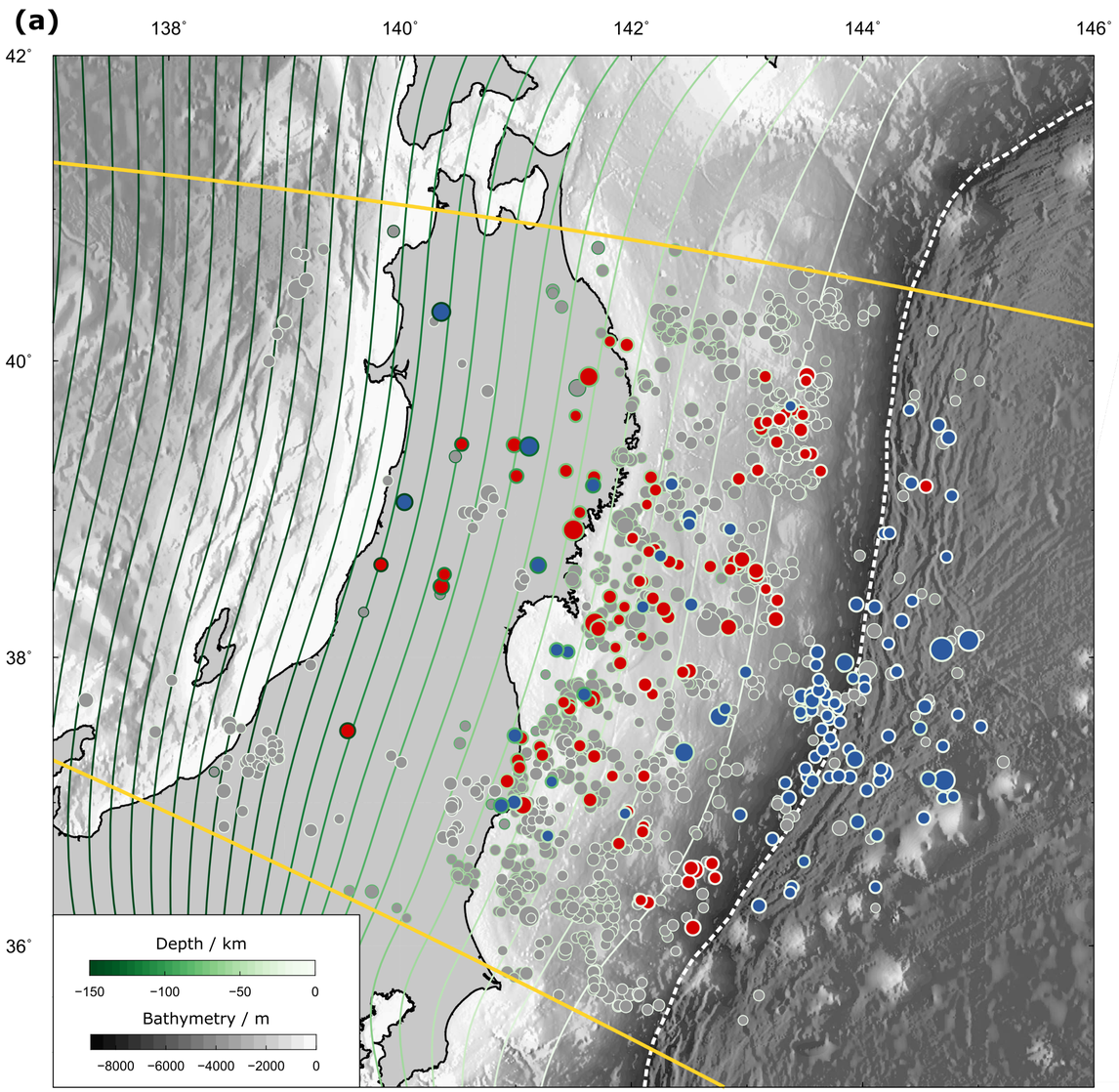

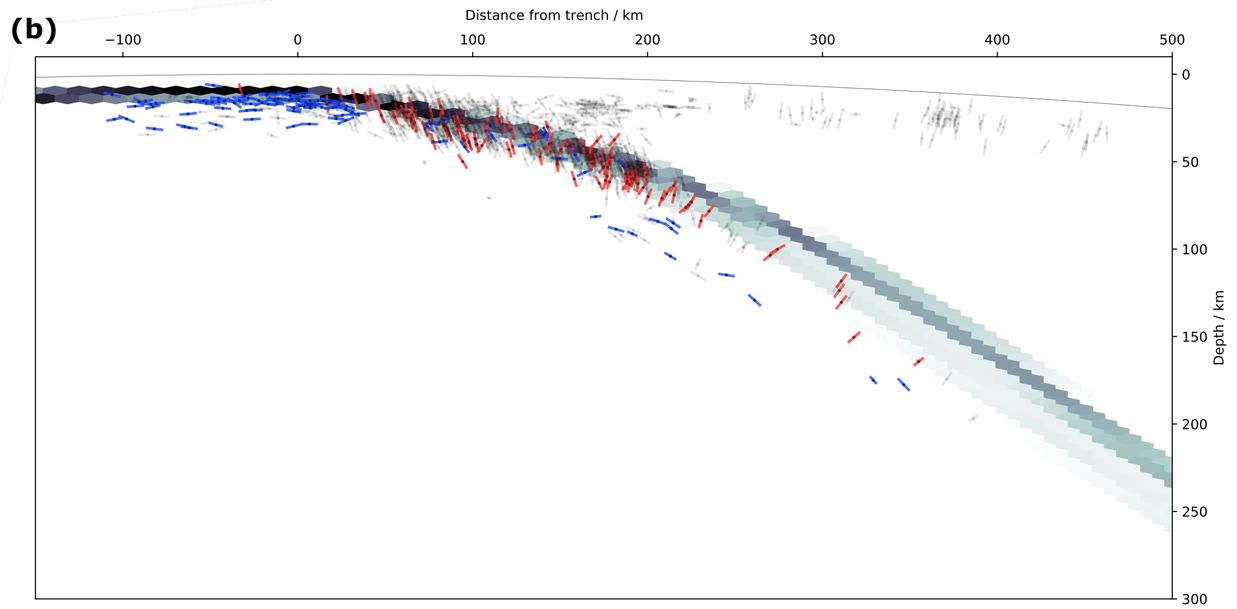

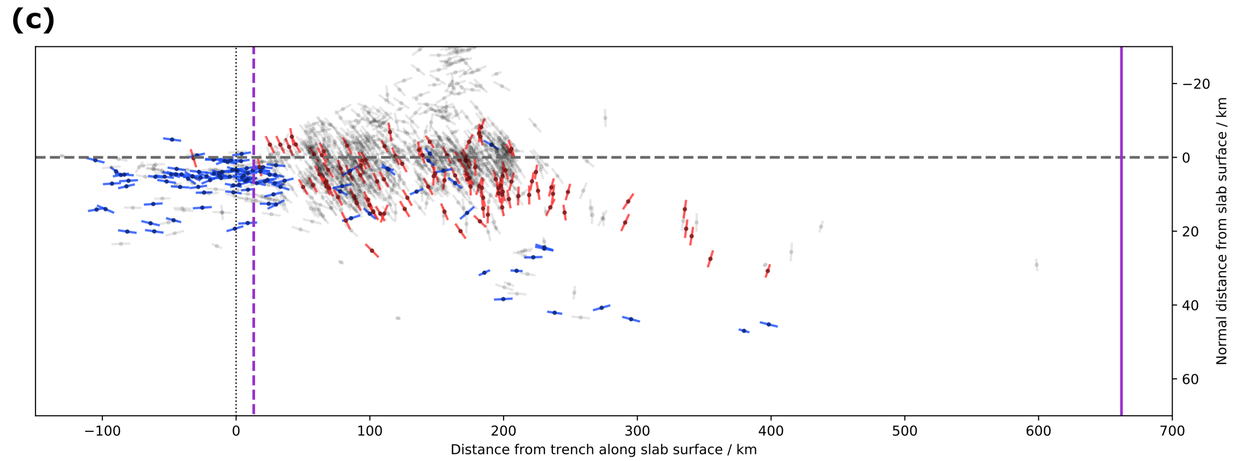

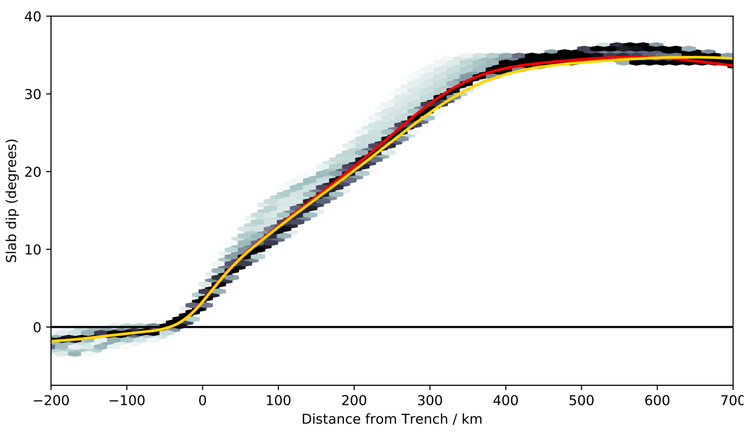

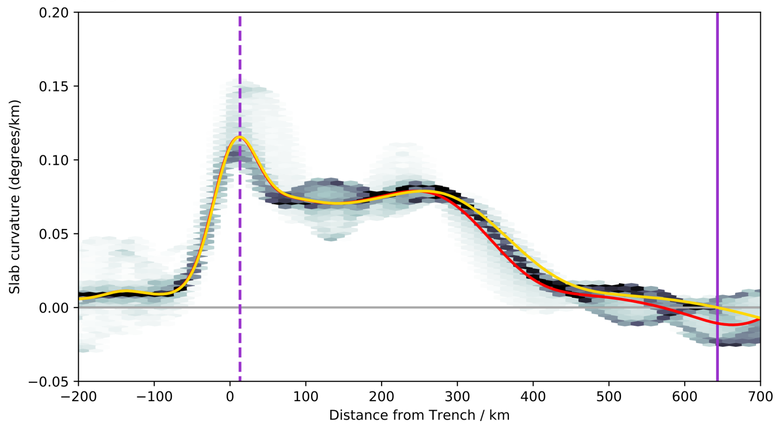

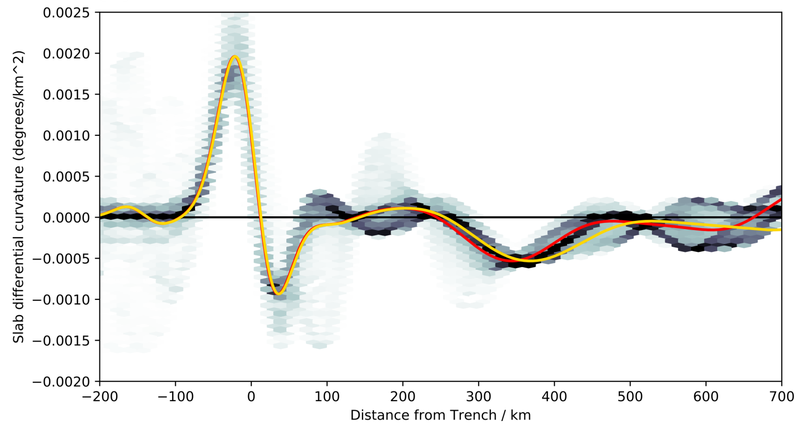

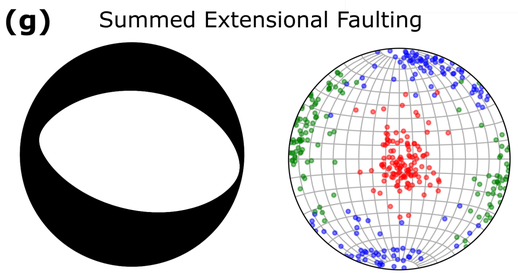

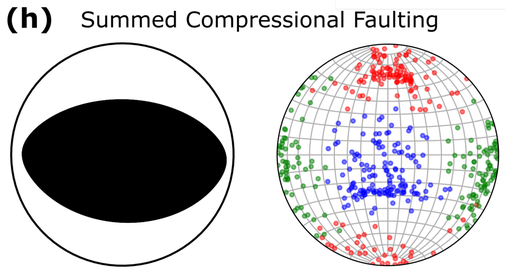

Extensional earthquake

Compressional earthquake

/ / P/N/T Axes

Mean (lateral distance from trench)

Mean (slab relative distance)

Peak mean curvature

1st zero-crossing of mean curvature

Figure 1.

(a)

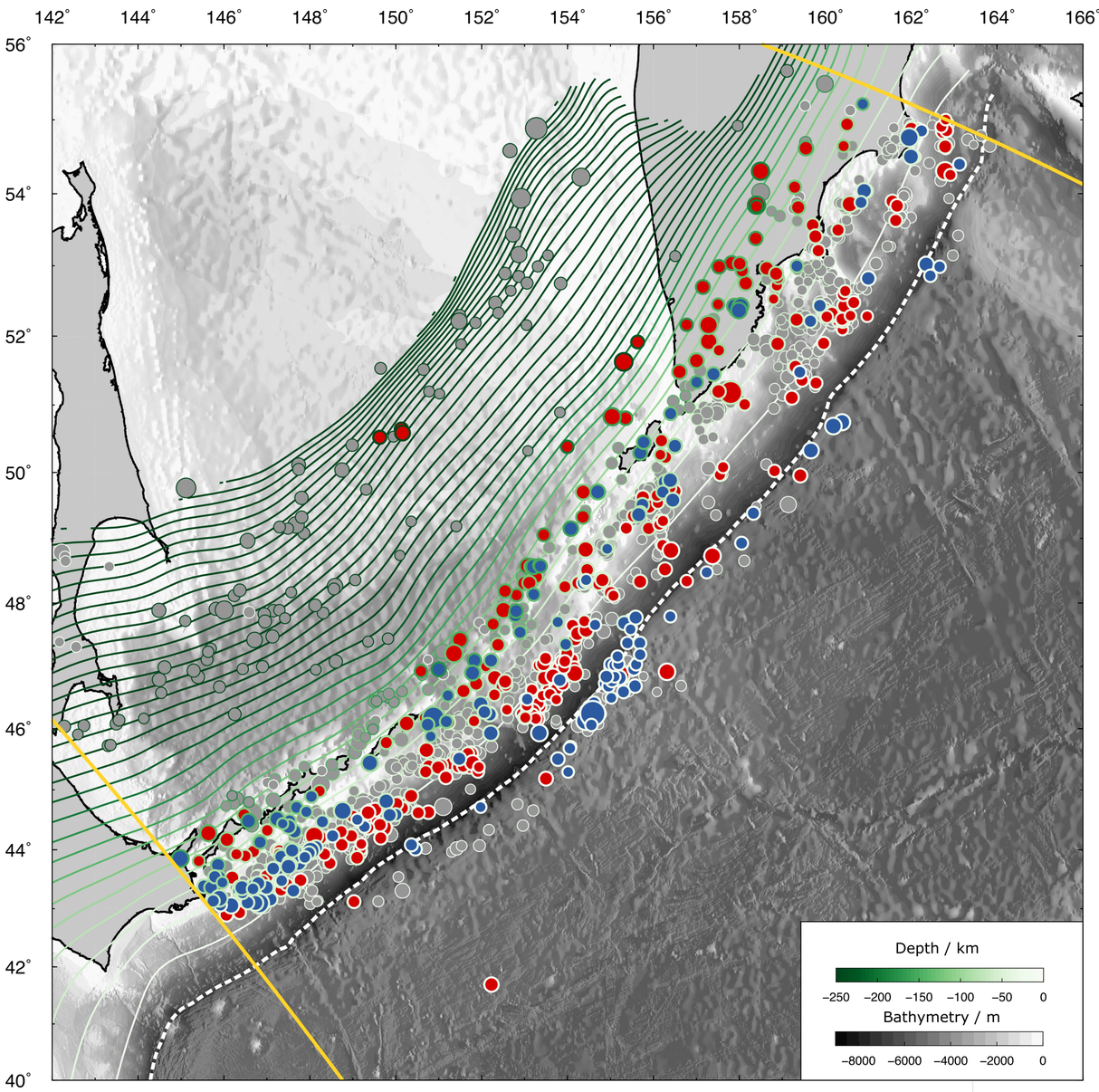

(b)

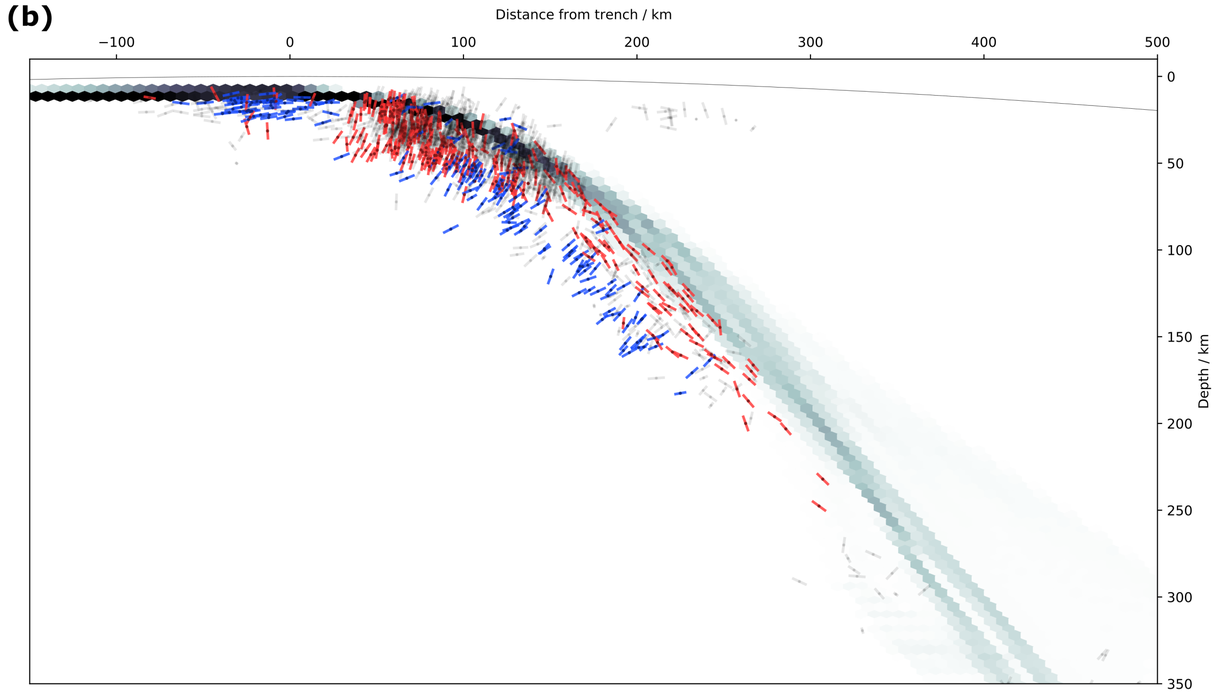

(c)

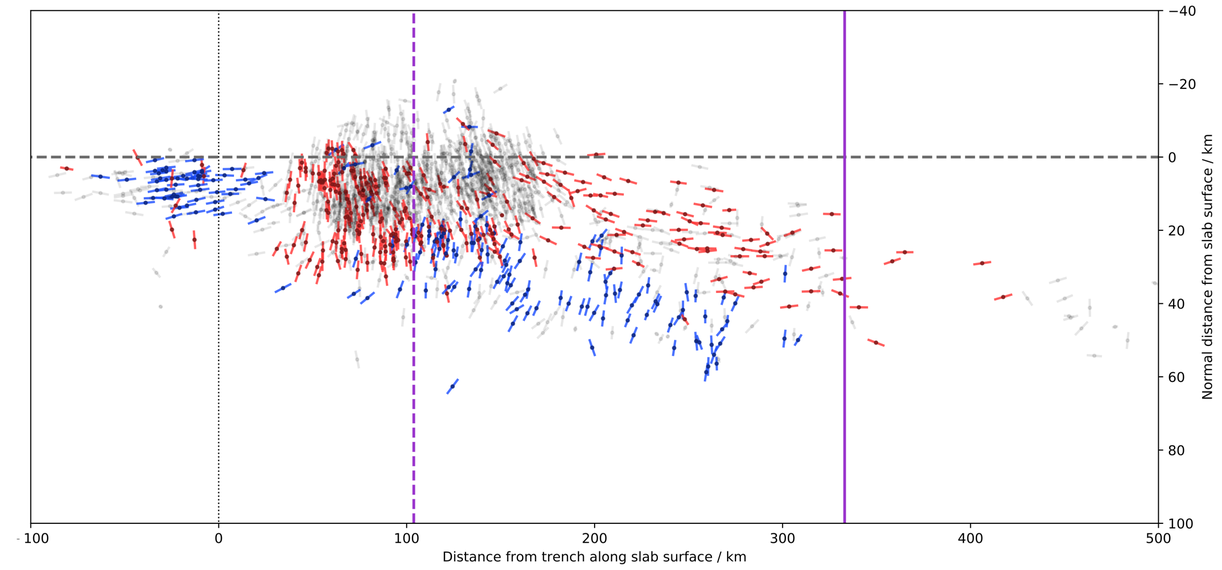

(d)

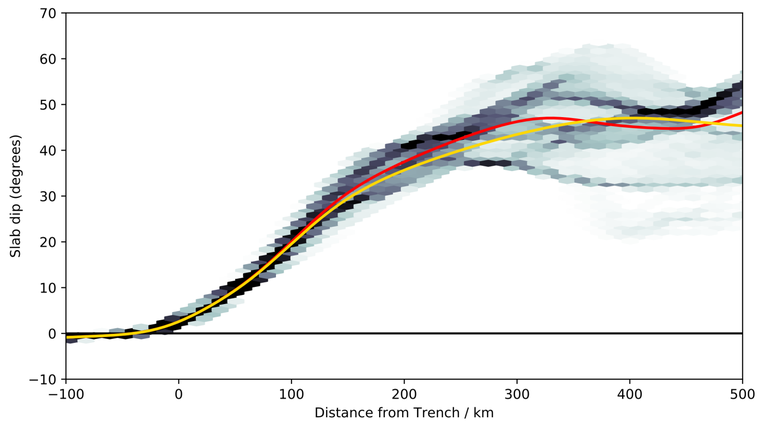

(e)

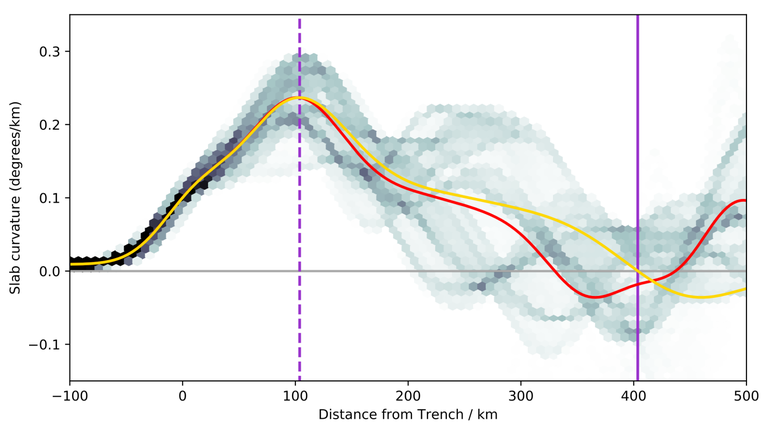

(f)

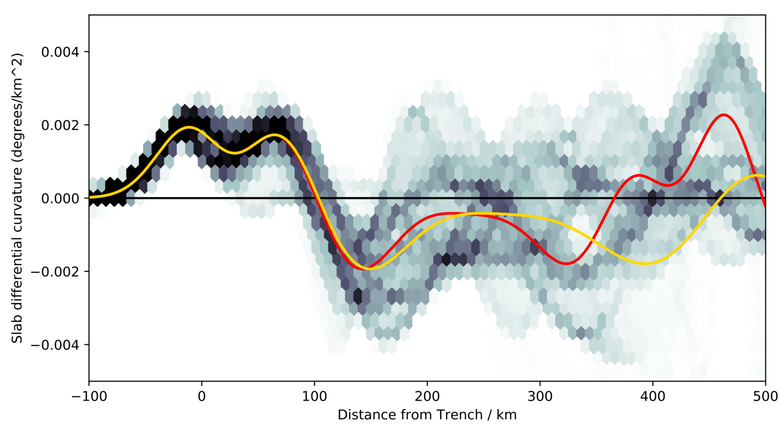

(g) Summed Extensional Faulting

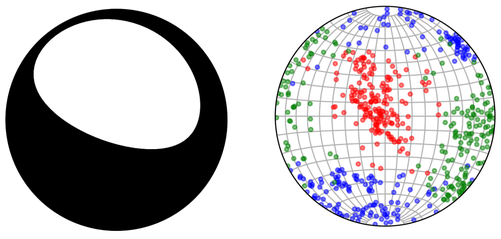

(h) Summed Compressional Faulting

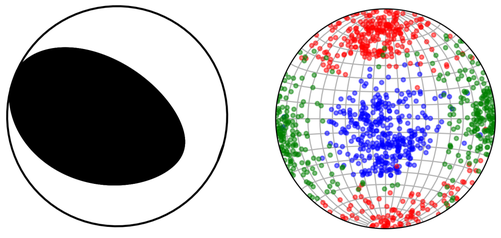

Extensional earthquake

Compressional earthquake

P/N/T Axes

Mean (lateral distance from trench)

Mean (slab relative distance)

Peak mean curvature

1st zero-crossing of mean curvature

Figure 3.

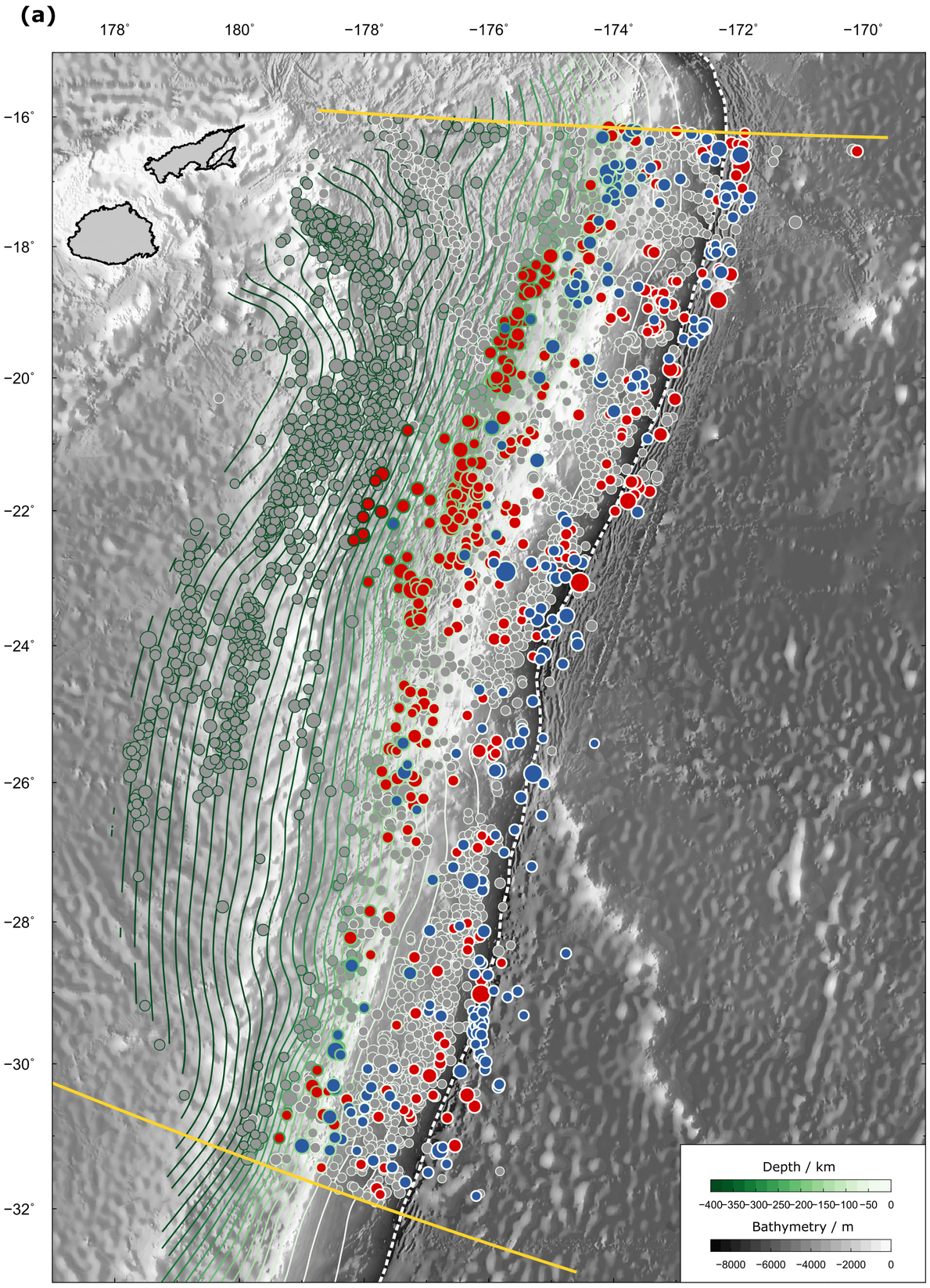
(a)
178˚
180˚
−178˚
−176˚
−174˚
−172˚
−170˚
−16˚
−18˚
−20˚
−22˚
−24˚
−26˚
−28˚
−30˚
−32˚
Depth / km
−400 −350 −300 −250 −200 −150 −100 −50 0
Bathymetry / m
−8000 −6000 −4000 −2000 0

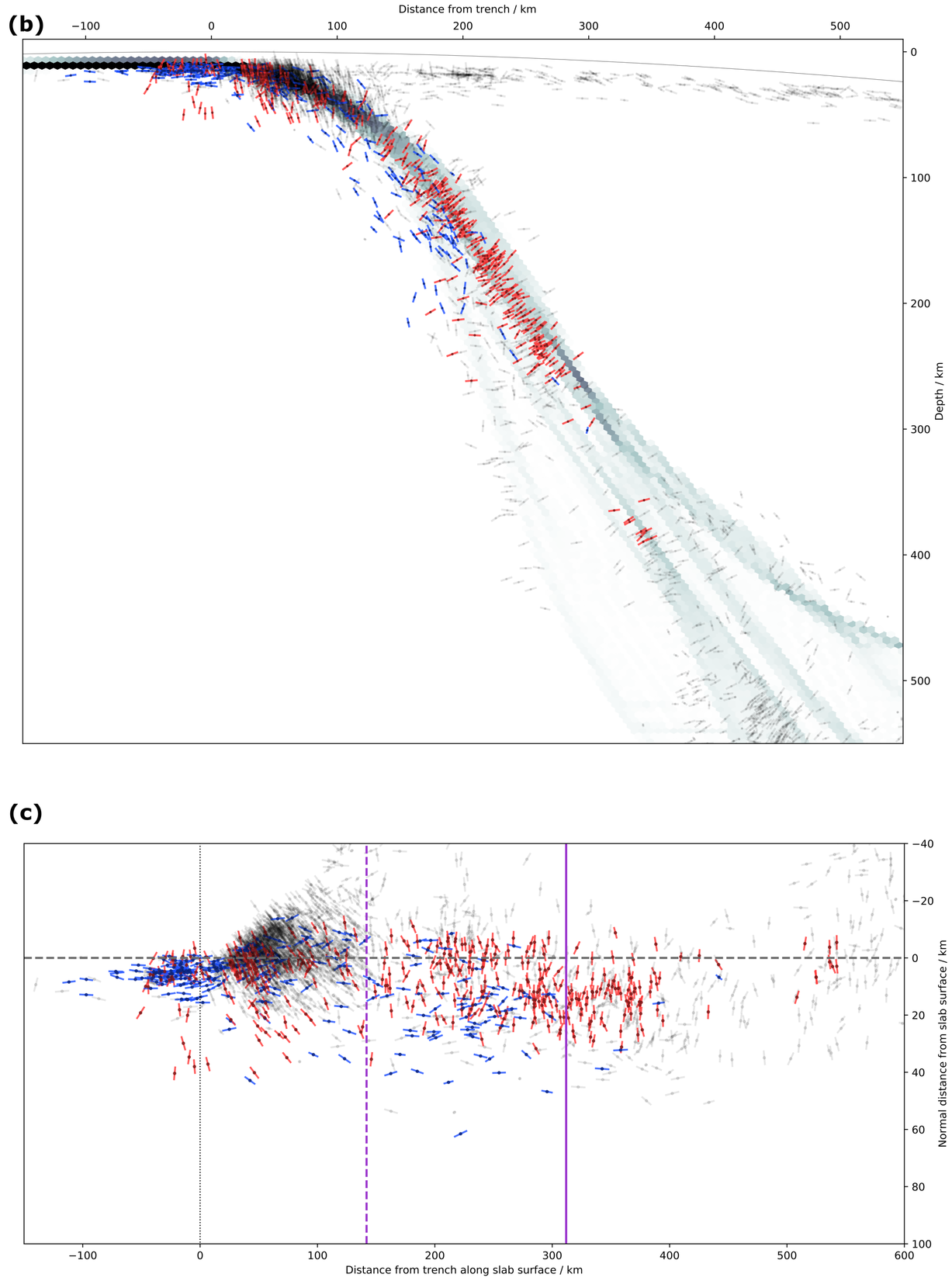
(b)
Distance from trench / km
−100 0 100 200 300 400 500
Depth / km
0 100 200 300 400 500
(c)
Normal distance from slab surface / km
−40 −20 0 20 40 60 80 100
Distance from trench along slab surface / km
−100 0 100 200 300 400 500 600

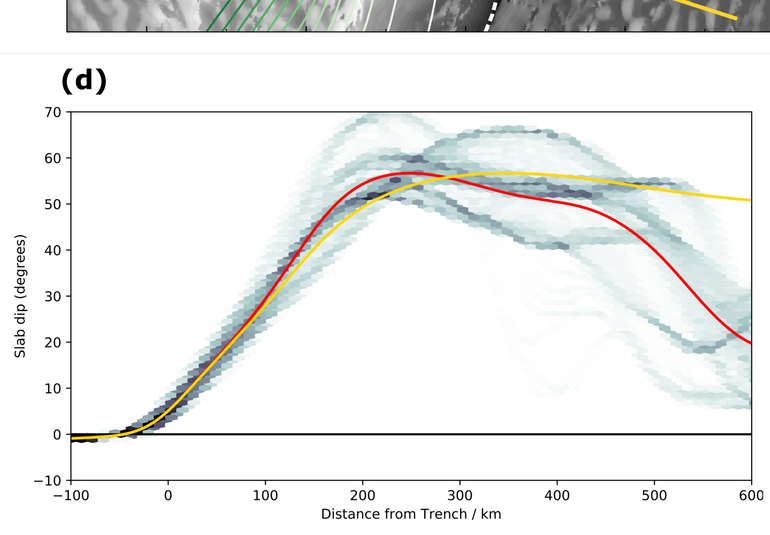
(d)
Slab dip (degrees)
70 60 50 40 30 20 10 0 −10
−100 0 100 200 300 400 500 600
Distance from Trench / km

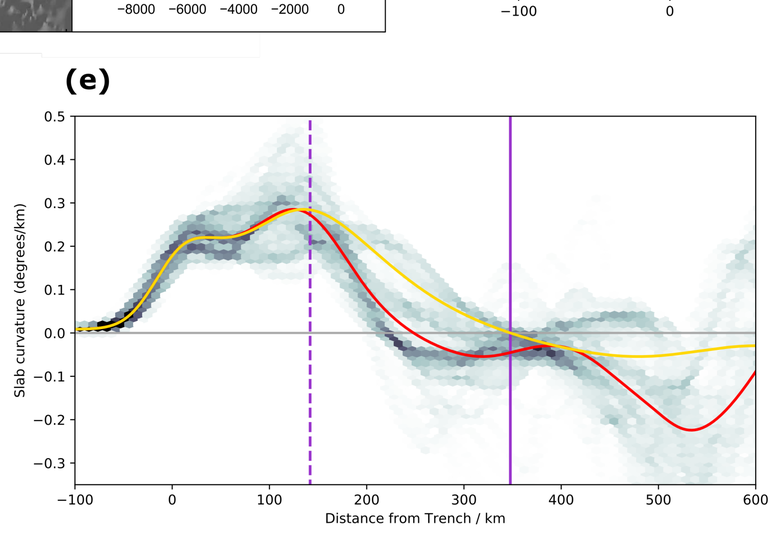
(e)
Slab curvature (degrees/km)
0.5 0.4 0.3 0.2 0.1 0.0 −0.1 −0.2 −0.3
−100 0 100 200 300 400 500 600
Distance from Trench / km

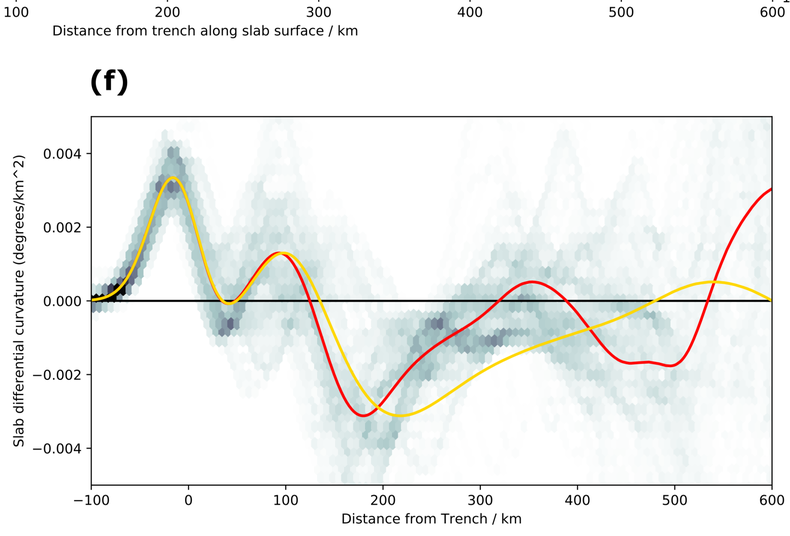
(f)
Slab differential curvature (degrees/km^2)
0.004 0.002 0.000 −0.002 −0.004
−100 0 100 200 300 400 500 600
Distance from Trench / km

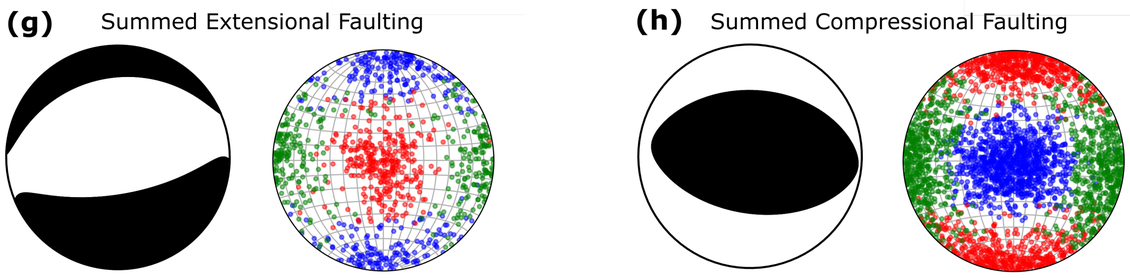
(g) Summed Extensional Faulting
(h) Summed Compressional Faulting
Extensional earthquake
Compressional earthquake
P/N/T Axes
Mean (lateral distance from trench)
Mean (slab relative distance)
Peak mean curvature
1st zero-crossing of mean curvature

Figure 4.

Separation based on rate-of-change in curvature

Total Seismic Moment / N·m

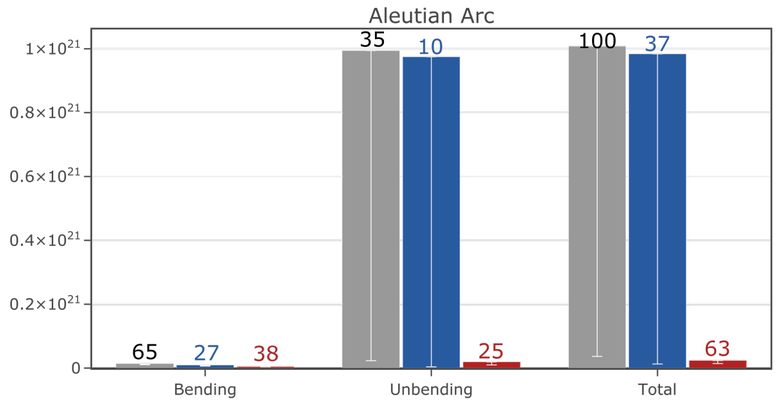

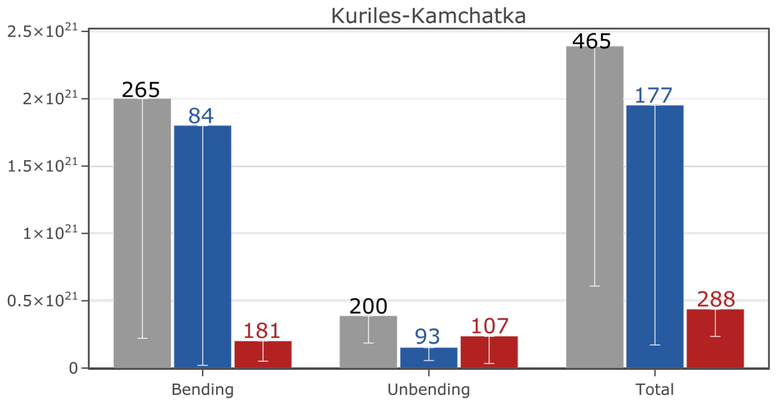

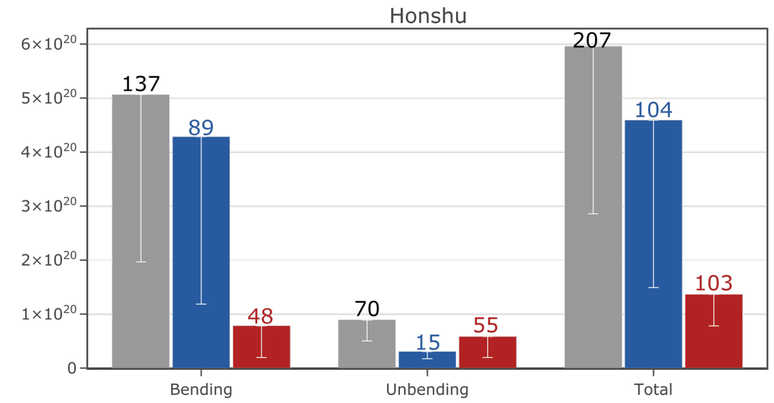

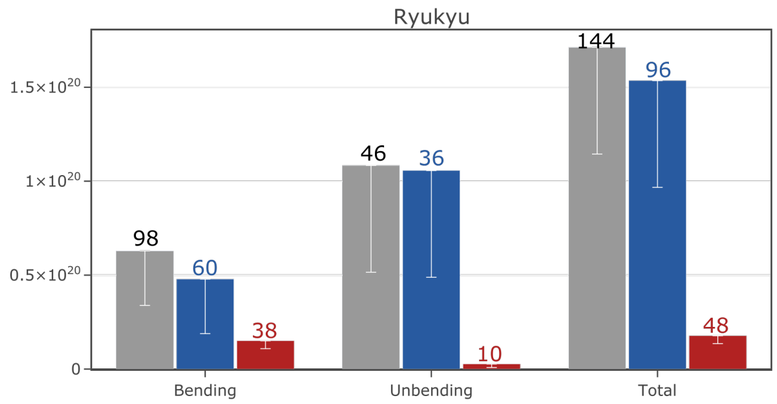

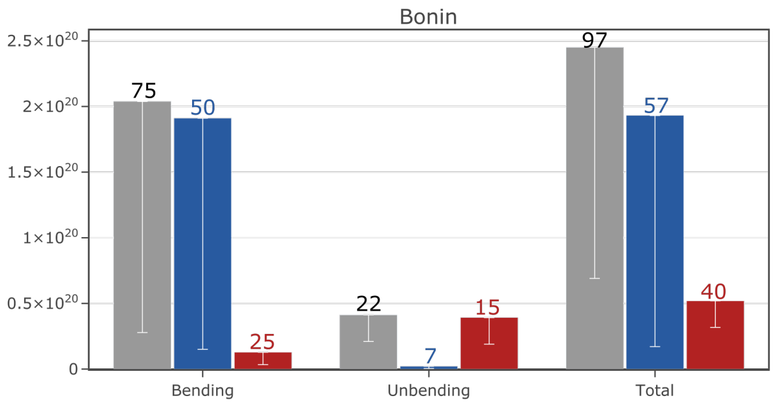

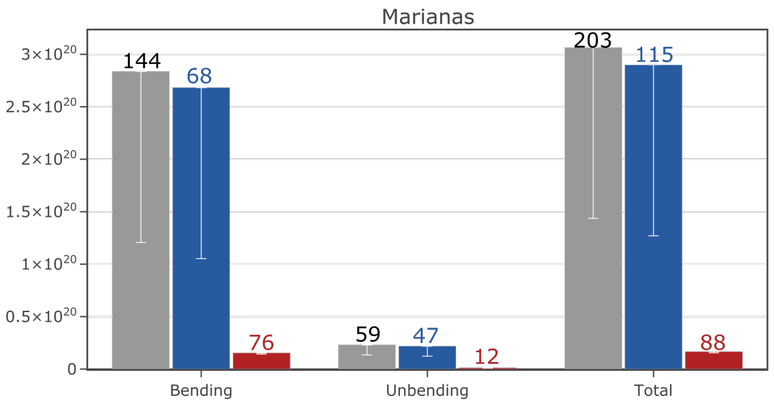

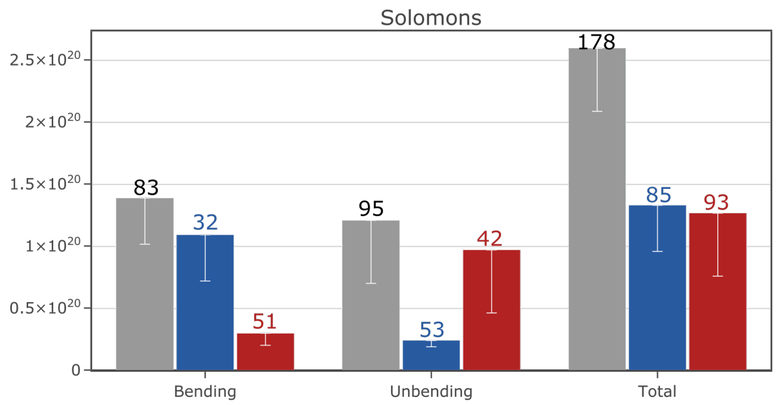

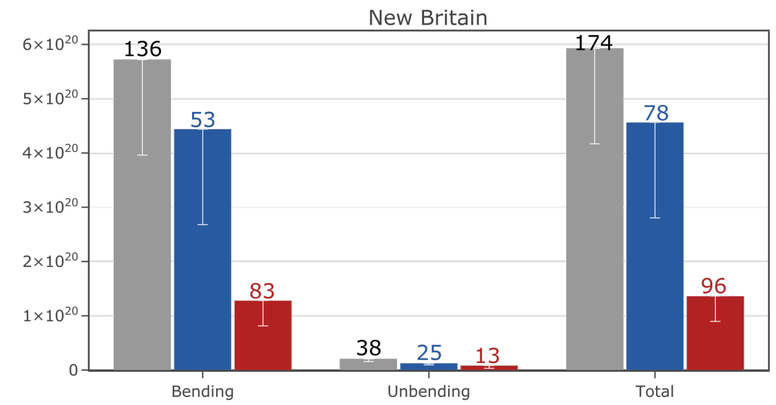

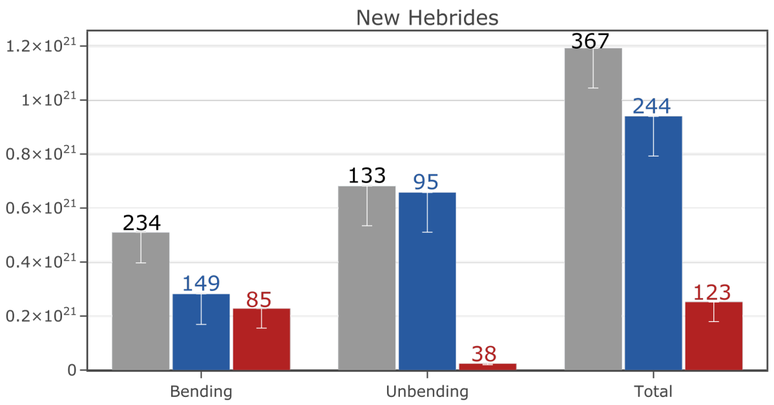

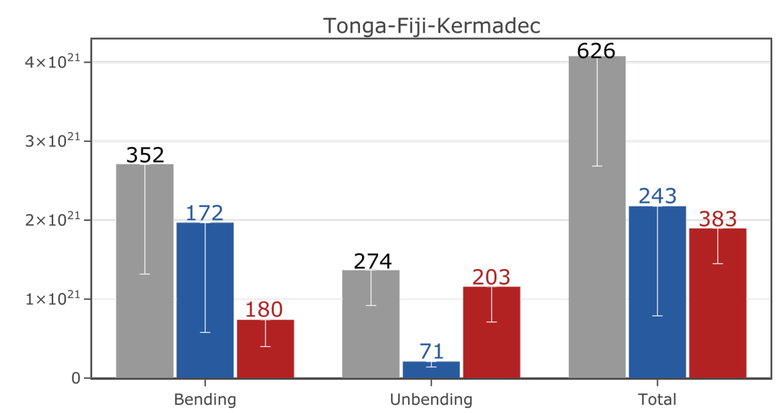

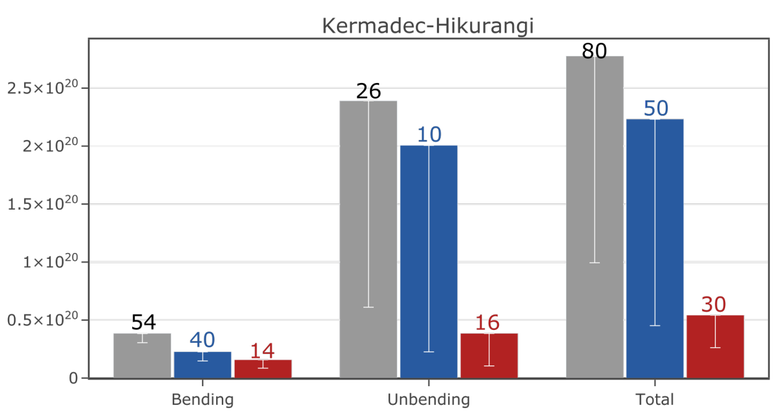

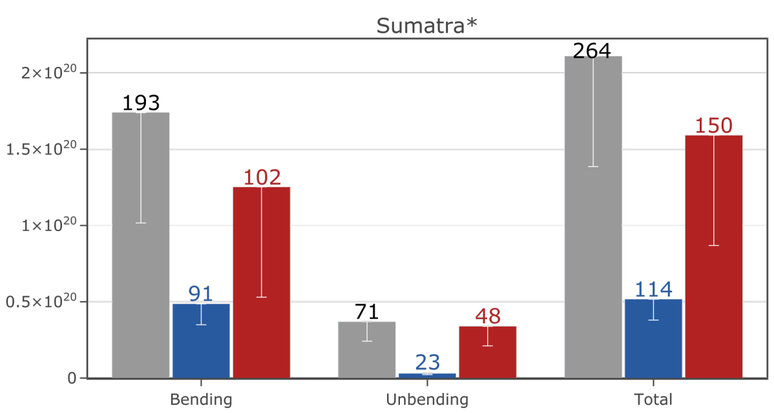

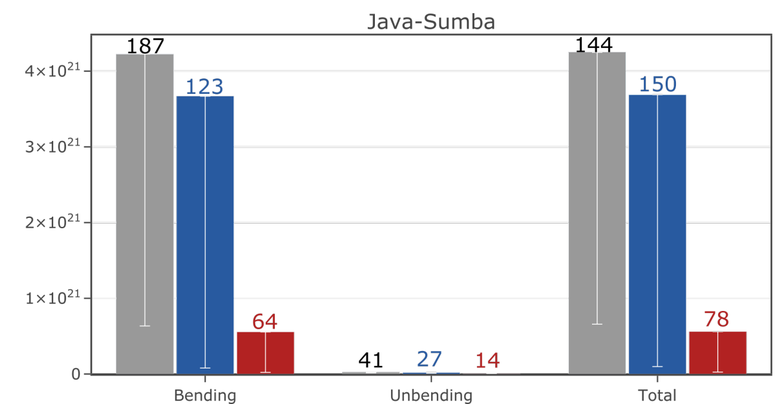

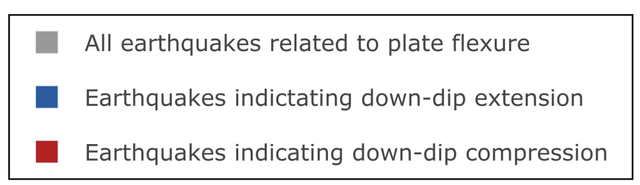

Figure 5.

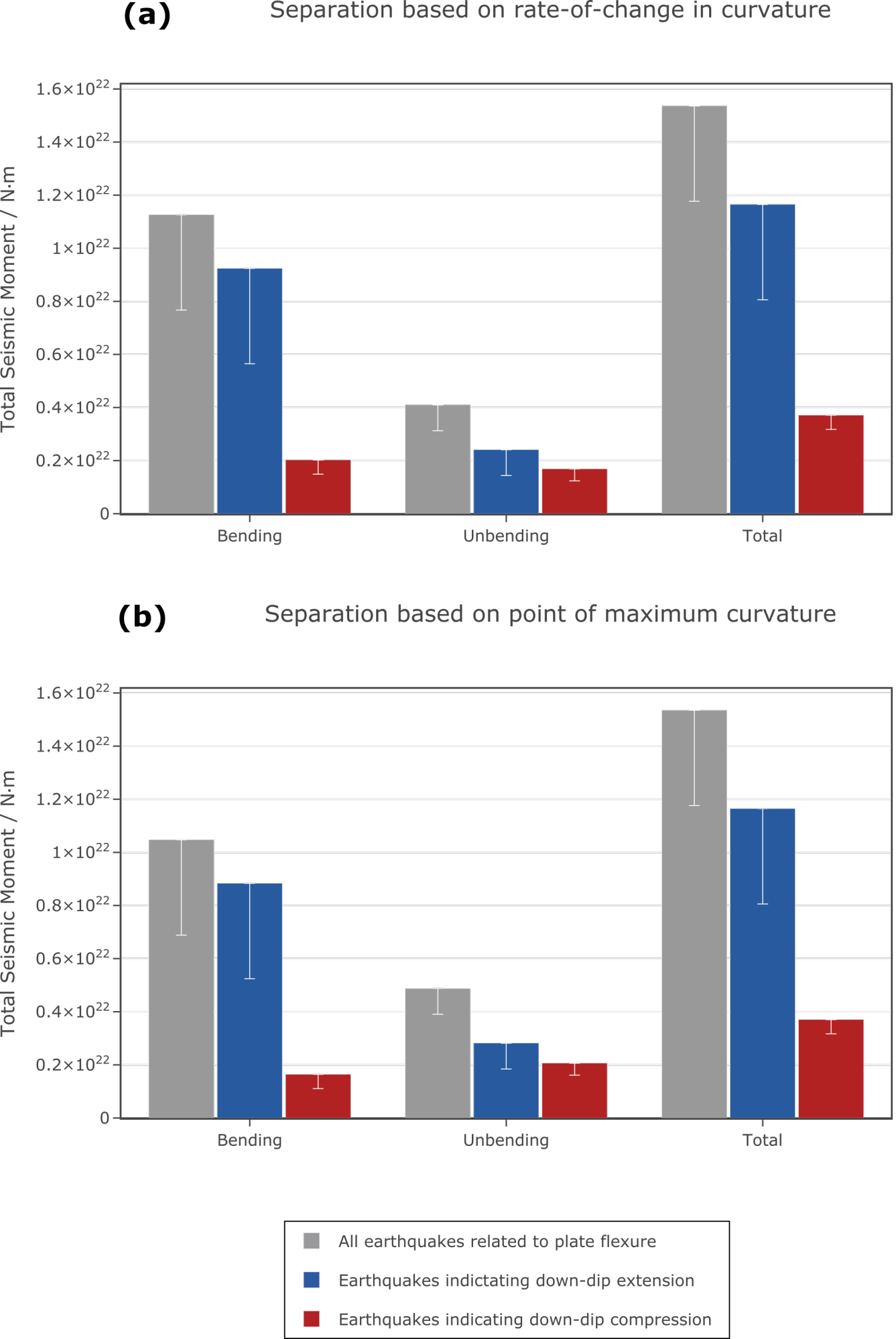
(a)
Separation based on rate-of-change in curvature
Total Seismic Moment / N·m
1.6×10^22
1.4×10^22
1.2×10^22
1×10^22
0.8×10^22
0.6×10^22
0.4×10^22
0.2×10^22
0
Bending
Unbending
Total
(b)
Separation based on point of maximum curvature
Total Seismic Moment / N·m
1.6×10^22
1.4×10^22
1.2×10^22
1×10^22
0.8×10^22
0.6×10^22
0.4×10^22
0.2×10^22
0
Bending
Unbending
Total
All earthquakes related to plate flexure
Earthquakes indictating down-dip extension
Earthquakes indicating down-dip compression

Figure 6.

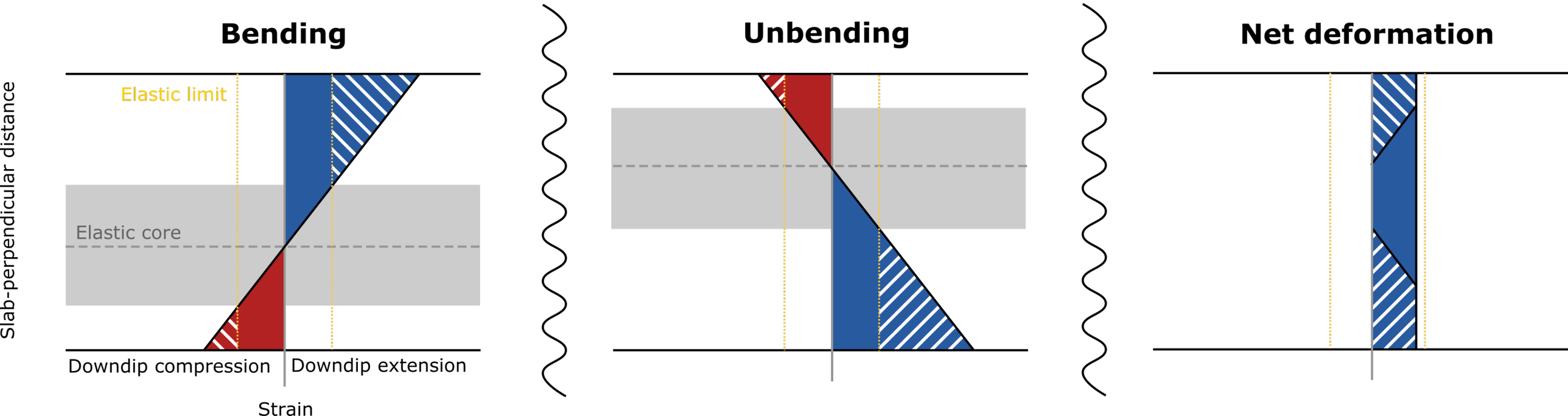
Bending
Unbending
Net deformation
Elastic limit
Elastic core
Slab-perpendicular distance
Downdip compression
Downdip extension
Strain